

รหัสโครงการ SUT7-706-54-12-70



รายงานการวิจัย

การวิเคราะห์กลไกการแยกตัวของอนุภาคผสมในฮอปเปอร์

(Analysis of Segregation Mechanism of Particle Mixtures in a Hopper)

ได้รับทุนอุดหนุนการวิจัยจาก
มหาวิทยาลัยเทคโนโลยีสุรนารี

ผลงานวิจัยเป็นความรับผิดชอบของหัวหน้าโครงการวิจัยแต่เพียงผู้เดียว

รหัสโครงการ SUT7-706-54-12-70



รายงานการวิจัย

การวิเคราะห์กลไกการแยกตัวของอนุภาคผสมในฮอปเปอร์ (Analysis of Segregation Mechanism of Particle Mixtures in a Hopper)

คณะผู้วิจัย

หัวหน้าโครงการ

Assistant Professor Dr. Boris Golman

สาขาวิชาวิศวกรรมเคมี

สำนักวิชาวิศวกรรมศาสตร์

มหาวิทยาลัยเทคโนโลยีสุรนารี

ได้รับทุนอุดหนุนการวิจัยจากมหาวิทยาลัยเทคโนโลยีสุรนารี ปีงบประมาณ พ.ศ. 2554

ผลงานวิจัยเป็นความรับผิดชอบของหัวหน้าโครงการวิจัยแต่เพียงผู้เดียว

กรกฎาคม 2556

Acknowledgement

The author would like to thank Suranaree University of Technology for their funding of this research. The assistance of the staff of Computer Center and students of the School of Computer Engineering of Suranaree University of Technology in simulation setup is highly appreciated. The author would like to acknowledge the many valuable suggestions made by Kunio Shinohara, Professor Emeritus of Hokkaido University.



(Assistant Professor Dr. Boris Golman)

Abstract

Whenever handling a mixture of particles with different properties, particles tend to segregate from each other during filling and withdrawal from vessels. In the present study, the segregation mechanisms are investigated in filling a hopper with binary-sized mixture of particles.

The discrete element method (DEM) is used for generation of segregation patterns during heap formation. Segregation profiles simulated by DEM are confirmed to be similar to ones obtained in experiments as well as calculated by the screening layer model. Thus, DEM models can be applied for generation of data to be used in the analysis of segregation mechanism in industrial apparatus.

The effects of particle mixture properties, process parameters, material properties and hopper geometry are investigated on the extent of segregation using the screening layer model. The segregation zones are found to be narrow for low initial mixing ratio and mixture feed rate, for longer heap flow length with higher penetration rate.

The detailed comparison of segregation patterns are made by changing operational conditions, particle properties and vessel dimensions in two and three dimensions. The operational conditions under consideration are the initial mixing ratio, mixture feed rate and heap flow length.

The results of the present analysis are intended to be used for understanding the segregation mechanism in filling hoppers utilized in various industries.

บทคัดย่อ

เมื่อไหร่ก็ตามที่การขนถ่ายของอนุภาคผสมที่มีความแตกต่างกันด้านคุณสมบัติของอนุภาค อนุภาคผสมเหล่านั้นมีแนวโน้มที่จะแยกออกจากอนุภาคอื่นๆในระหว่างการบรรจุหรือการนำออกจากภาชนะบรรจุ ในงานวิจัยนี้กลไกการแยกตัวของอนุภาคผสมสองขนาดที่บรรจุลงฮอปเปอร์ได้ถูกทำการศึกษา

วิธีดิสครีทเอลิเมนต์ (Discrete element method DEM) ถูกใช้สำหรับการก่อกำเนิดของรูปแบบการแยกตัวของอนุภาคในระหว่างการก่อรูปฮอป ผลของแบบจำลองรูปแบบการแยกตัวโดยวิธีดิสครีทเอลิเมนต์รวมถึงผลการคำนวณด้วยการใช้แบบจำลองสกรีนนิ่งเลเยอร์ (Screening layer model) ยืนยันได้ว่ามีความเหมือนกันกับผลที่ได้ในการทดลอง ดังนั้นแบบจำลองวิธีดิสครีทเอลิเมนต์สามารถประยุกต์ใช้สำหรับการก่อกำเนิดข้อมูลเพื่อใช้ในการวิเคราะห์กลไกการแยกตัวในอุปกรณ์ทางด้านอุตสาหกรรมได้

ผลกระทบของคุณสมบัติของอนุภาคผสม ตัวแปรต่างๆของกระบวนการ คุณสมบัติของวัสดุ และโครงสร้างของฮอปเปอร์ ได้ถูกศึกษาในขอบเขตของการแยกโดยใช้แบบจำลองสกรีนนิ่งเลเยอร์ โชนของการแยกถูกพบว่า จะแคบสำหรับอัตราส่วนการผสมเริ่มต้นและอัตราการป้อนของผสมที่น้อย และสำหรับความยาวการไหลฮอปที่มากกว่าด้วยอัตราการแทรกผ่านที่สูงกว่า

การเปรียบเทียบรายละเอียดของรูปแบบการแยก ถูกทำโดยการเปลี่ยนสภาวะปฏิบัติการต่างๆ การเปลี่ยนคุณสมบัติของอนุภาค และการเปลี่ยนขนาดของอุปกรณ์ที่บรรจุ ในสองและสามมิติ สภาวะปฏิบัติการภายใต้ความสนใจคือ อัตราส่วนผสมเริ่มต้น อัตราการป้อนของผสม และความยาวการไหลฮอป

ผลของการวิเคราะห์จากการศึกษานี้ มีจุดประสงค์ที่จะใช้สำหรับการทำความเข้าใจกลไกการแยกในอุตสาหกรรมที่หลากหลายที่มีการใช้งานการบรรจุอนุภาคในฮอปเปอร์

Contents

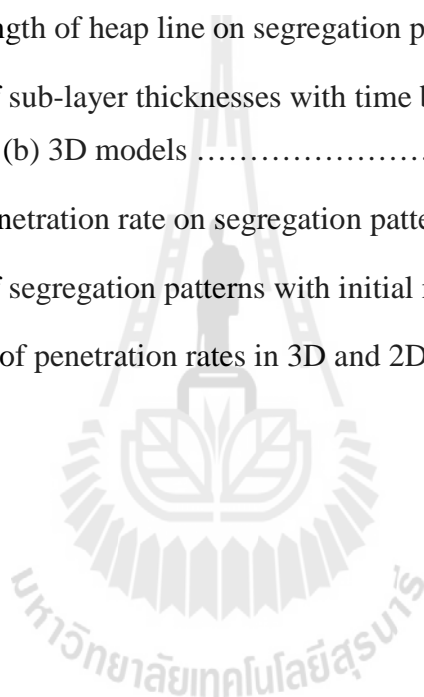
Acknowledgment	I
Abstract	II
Contents	IV
List of Figures	VI
List of Tables	VIII
1. Introduction	
1.1 Literature review	1
1.2 Aims of this research	3
1.3 Scope of research	3
2. Theory	
2.1 Theoretical background of discrete element method	4
2.1.1 Outline of discrete element method	4
2.1.2 Contact detection	4
2.1.3 Force balances	8
2.1.4 Contact forces	9
2.2 Theoretical background of screening layer model	13
2.2.1 Outline of screening layer model	13
2.2.2 Derivation of balance equations in two dimensions	15
2.2.3 Velocity of flowing sub-layers	17
2.2.4 Penetration rate	18
2.2.5 Balance equations in three dimensions	22
3. Simulation	
3.1 Particle mixture definition	24

3.2 Setup of discrete element simulations	24
4. Results and Discussions	
4.1 Simulation results by discrete element method	28
4.1.1 Calibration of simulation model	28
4.1.2 Segregation simulation results by DEM	30
4.2 Calculation results by screening layer model	34
4.2.1 Model calibration	34
4.2.2 Effect of process parameters on segregation of binary mixture	37
Definition of operational and flowability parameters	37
Typical profiles of mixing ratio and flowing sub-layer thicknesses.	38
Effect of penetration and packing rates	40
Effect of velocity ratio	41
Influence of operational parameters	42
Influence of hopper geometry parameters	43
4.2.3 Comparison of segregation patterns in two and three dimensions	43
5. Conclusions	48
References	49

List of Figures

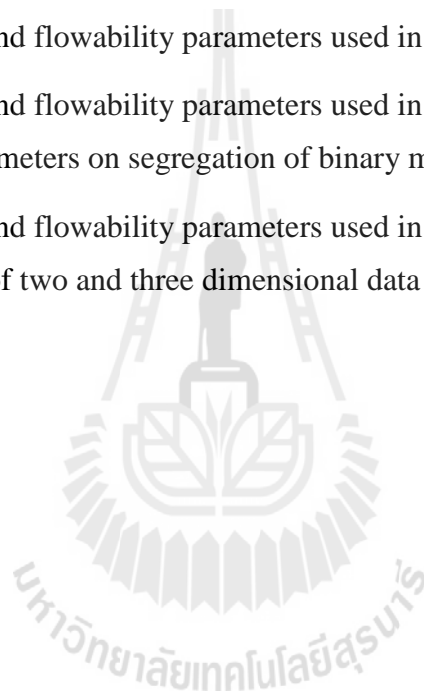
Figure 1. Flowchart of DEM algorithm	5
Figure 2. Coordinates and displacements of a disk element	6
Figure 3. Contact of two particles	6
Figure 4. Contact of a particle with wall	7
Figure 5. Derivation of particle-wall contact	8
Figure 6. Illustration of dashpot-slider model	9
Figure 7. Illustration of screening layer model	14
Figure 8. Experimental two-dimensional system for measuring particle segregation	25
Figure 9. Two-dimensional simulation setup	25
Figure 10. Illustration of measuring positions along the heap line	27
Figure 11. Illustration of measurement of angle of repose.....	28
Figure 12. Effect of coefficient of rolling friction on particle heap formation: (a) 0.1, (b) 0.2, (c) 0.3, (d) 0.4, (e) 0.5	29
Figure 13. Snapshots of two-dimensional simulation results for various initial concentrations of fine component: (a) 0.01, (b) 0.1, (c) 0.3	31
Figure 14. Distribution of segregating component along heap line: (a) 0.01, (b) 0.1, (c) 0.3	32
Figure 15. Variation of segregation index with initial concentration of segregating component	33
Figure 16. Validation of two-dimensional screening layer model by fitting experimental data	34
Figure 17. Validation of three-dimensional screening layer model by fitting experimental data	35
Figure 18. Variation of mixing ratio with time	38

Figure 19. Variation of thicknesses of flowing sub-layers with time: (a) segregating, (b) separating, (c) remained	39
Figure 20. Effect of penetration rate on segregation profile	40
Figure 21. Effect of packing rate on segregation profile	41
Figure 22. Effect of velocity ratio on segregation profile	41
Figure 23. Effect of initial mixing ratio on segregation profile	42
Figure 24. Effect of feed rate on segregation profile	42
Figure 25. Effect of length of heap line on segregation profile	43
Figure 26. Variation of sub-layer thicknesses with time by (a) 2D and (b) 3D models	45
Figure 27. Effect of penetration rate on segregation pattern	46
Figure 28. Variation of segregation patterns with initial mixing ratio	47
Figure 29. Correlation of penetration rates in 3D and 2D	47



List of Tables

Table 1. Initial conditions for particle generation in two dimensional simulation	26
Table 2. Material and flow properties of particles and walls	26
Table 3. Angle of repose in heap formed with various coefficients of rolling friction	30
Table 4. Operational and flowability parameters used in 2D model validation	34
Table 5. Operational and flowability parameters used in 3D model validation	36
Table 6. Operational and flowability parameters used in study on effect of process parameters on segregation of binary mixture	37
Table 7. Operational and flowability parameters used in comparison of two and three dimensional data	44



1. Introduction

1.1 Literature review

Segregation of particles different in properties such as size, density and shape are industrially important in storage, supply and reaction of chemicals, pharmaceuticals, food and agricultural products, from the viewpoint of uniform mixture of processing materials, high contact efficiency and of constant withdrawal rate (Bates, 1997).

Segregation of particle mixtures often results in quality control problems due to the waste of raw materials, loss of production, as well as increased maintenance and capital costs required to modify existing facilities. The cost implications can be great, even when handling small quantities of material (McCarthy, 2009).

However, the design of industrial equipment with the objective of avoiding segregation phenomena is based mainly on manufacturer's operational experience rather than on theoretical considerations (Tang et al., 2004). The major problems are associated with the insufficient understanding of segregation mechanisms of particle mixture influenced by process parameters, vessel geometry and particle properties (McCarthy, 2009) as well as difficulties associated with experimental study of segregation pattern in a three-dimensional segregation tester (Shinohara and Enstad, 1990) owing to the necessity of taking large number of powder samples without disturbing the heap structure.

Segregation or separation of granular materials has been a focus of academic study for many decades (Shinohara, 2006; Williams, 1976). Much of the early works in this area were the experimental studies to identify the source of segregation in a specific unit operation. For example, some of the initial studies were of segregation issues related to the coal (Mitchell, 1938), mining and metallurgy (Seaton, 1960) industries. There are some reports in literature on segregation during handling of powder mixture in various apparatus, such as tumblers (Campbell and Bauer, 1966), fluidized-beds (Hoffmann, 1993), mixers (Cleary, 1998), hoppers (Shinohara et al., 2002; Shinohara and Golman, 2003), moving-beds (Shinohara and Shoji, 1970; Shinohara and Golman, 2002; Shinohara et al., 2007), and during the gravity-driven flow of powder in a vertical pipe (Liss et al, 2004).

In recent years, researchers began to turn their efforts toward the classification of segregation mechanism and as many as 13 different segregation mechanisms are quoted in the literature (Silva et al., 2000). Among them, four mechanisms were recognized as most important ones in formation of segregation profiles, i.e. percolation/sieving, fluidization, convection, and trajectory segregation (Shinohara et al., 1972). Sometimes it is not easy to identify the primary mechanism of segregation.

Shinohara [Shinohara *et al.*, 1972, Shinohara and Miyata, 1984] developed a screening layer model to analyze the segregation phenomena during heap formation in a two-dimensional tester. This model was extended to three-dimensional heaps [Shinohara and Enstad, 1990, Rahman *et al.*, 2011], multi-feed blast furnace [Shinohara and Saitoh, 1993] and moving-bed [Shinohara and Golman, 2002].

Recently, the discrete element method was applied for simulation of industrial particle flows (Cleary, 2000). The trajectories, spins and orientations of all particles are followed as well as their interactions with other particles. Equations of motion are also solved for the boundary objects with which the particles interact, i.e. hopper walls. The discrete element method has been successfully applied to many practical applications, including ball-mills (Mishra and Rajamani, 1992), fluidized-beds (Tatemoto et al., 2004), mixer-granulator (Gannt and Gatzke, 2005) and hoppers (Ketterhagen, 2010).

Therefore, there is a need to identify mechanisms of segregation of particle mixtures during filling hoppers and to study effects of process and hopper geometry parameters on the extent of segregation by using the screening layer model that utilizes data collected in two-dimensional experiments as well as data generated through the detail modeling of particle interactions using the discrete element method.

1.2 Aims of this research

The objectives of the present research are:

- to apply the discrete element method for generation of segregation patterns of particle mixture during filling hoppers
- to study the effects of particle mixture properties, process parameters, material properties and hopper geometry on intensity of segregation of particle mixture

- to compare segregation patterns in two- and three dimensions by changing the operational conditions, particle properties and vessel dimensions as a part of recent research efforts aimed at prediction of segregation behavior of particle mixture in industrial three-dimensional apparatus using experimental data collected in the two-dimensional segregation tester.

1.3 Scope of research

The present research is limited to the analysis of segregation behavior of the binary mixture of particles of various sizes. The density and the shape of the particles are assumed to be constant.

The discrete element method will be adopted to simulate the heap formation during filling hoppers. The model will be calibrated by comparison of simulated angle of repose of coarse particles in the heap with experimental one. The segregation profiles will be related quantitatively with ones calculated by the screening layer model.

The effects of the initial mixing ratio of fine particles, feed rate of particle mixture, penetration and packing rates, velocity ratio and hopper width will be investigated on the extent of segregation of particle mixture by the screening layer model.

The segregation profiles in two- and three dimensions will be compared for various initial mixing ratios of fine particles and other particle properties, such as the size ratio, flowability, void fraction and angle of repose, by changing the penetration rate of fine particles to the heap surface through voids formed among framing course particles during descending of particle mixture along the heap line.

2. Theory

2.1 Theoretical background of discrete element method

2.1.1 Outline of discrete element method

A new promising approach to the modeling of particle flow was developed in the last ten years based on the discrete element method (DEM) (Cundall and Strack, 1979). It provides a way of simulating particle flow by modeling an interaction of each particle with the surrounding particles. The basic assumption of DEM is that in a particulate system forces are only acting between particles being directly in contact.

The DEM simulates displacement and rotation of discrete particles which interact with their nearest neighbors through local contact laws. Particles are constantly separated from each other and formed new contacts as the calculation advances.

Therefore, the DEM simulation is essentially consists of the three major steps:

1. contact detection
2. contact processing
3. particle motion

The DEM flowchart is shown in Fig. 1.

The coordinates and displacements of a particle, a disk element in the two dimensions or a sphere in three dimensions, are shown in Fig. 2. The position and orientation of the i^{th} disk is described by the disk center coordinates O_i and the rotational angle θ_i .

2.1.2 Contact detection

The search for the contacts between particles is performed by detecting the distance between a particle and its neighboring particles, as illustrated in Fig. 3. A contact between particles i and j is registered when an overlap between two particles is detected, i.e. the distance between their centers is less than the sum of their radii.

$$R_{ij} = \sqrt{(x_i - x_j)^2 + (y_i - y_j)^2} \leq r_i + r_j \quad (1)$$

where R_{ij} is the distance between particle centers, (x_i, y_i) and (x_j, y_j) are the center coordinates of particles i and j , and r_i and r_j are their radii, respectively.

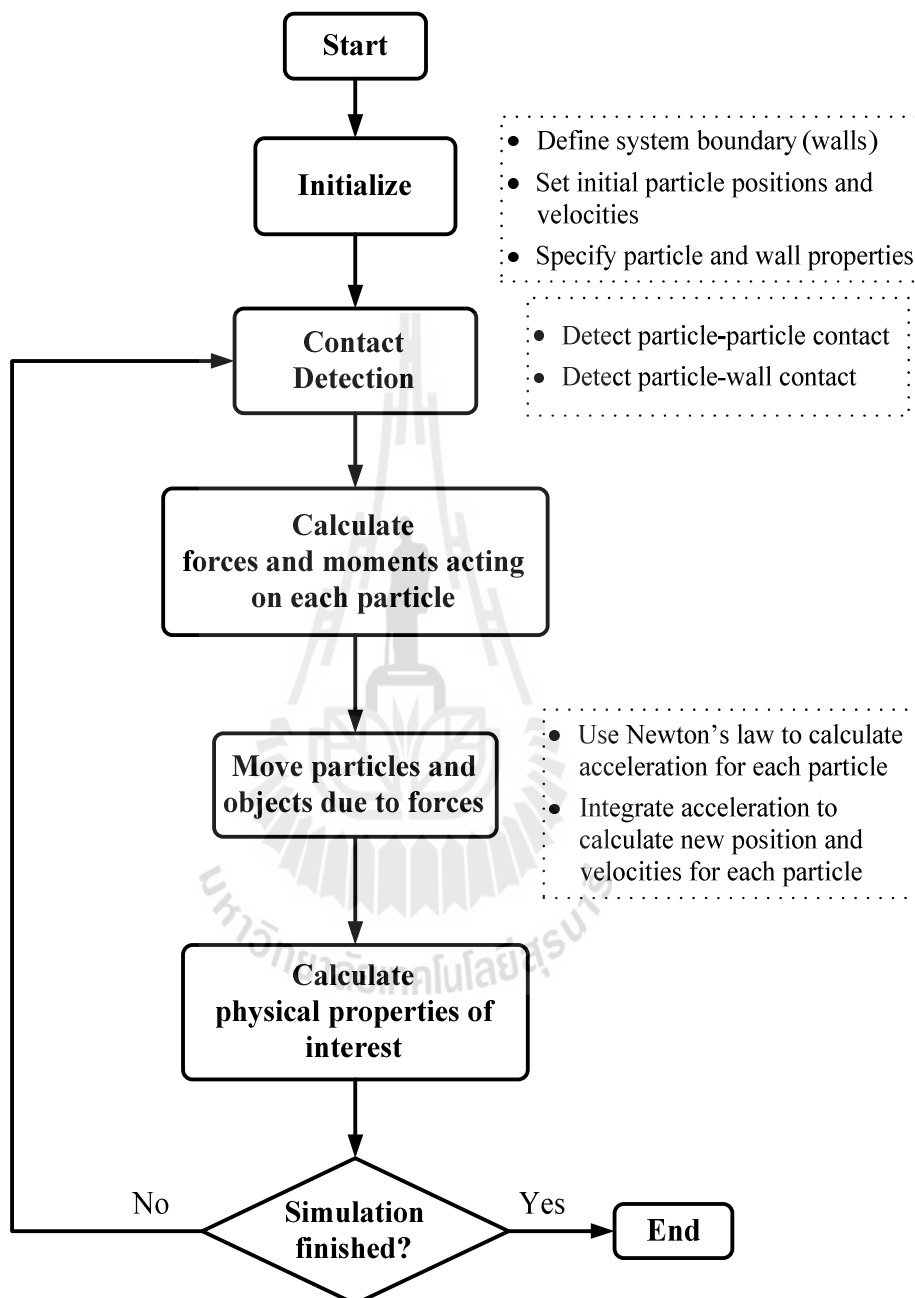


Figure 1. Flowchart of DEM algorithm

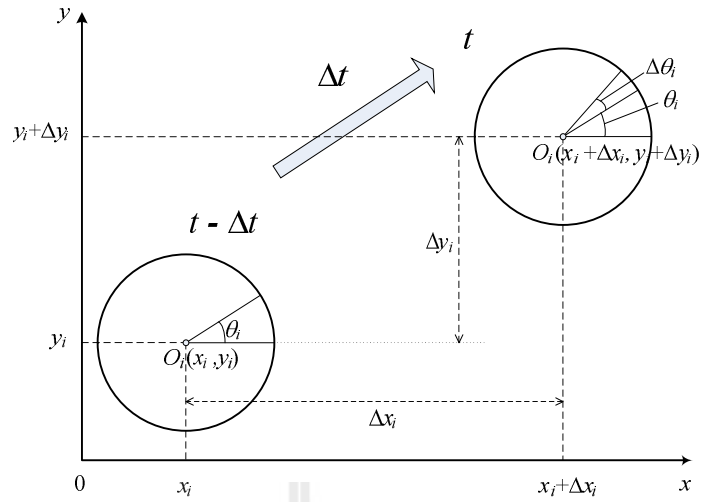


Figure 2. Coordinates and displacements of a disk element

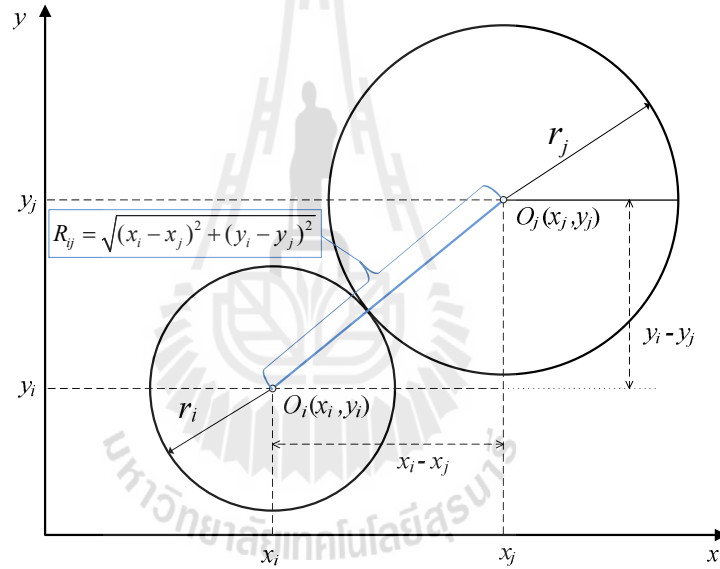


Figure 3. Contact of two particles

The detection of contact between particle and wall is carried out in a similar way to the particle-particle contact. A typical wall with straight rigid boundaries is defined in terms of fixed initial and end positions with coordinates (x_0, y_0) and (x_1, y_1) , respectively. Thus, the wall length L and orientation angle θ with respect to the x axis (counterclockwise) are

$$L = \sqrt{(x_1 - x_0)^2 + (y_1 - y_0)^2} \quad (2)$$

$$\cos \theta = (x_1 - x_0) / L; \sin \theta = (y_1 - y_0) / L, \quad (3)$$

as shown in Fig. 4.

The distances between the particle center (x_i, y_i) and the wall in directions parallel to the wall and perpendicular to the wall are denoted by s_h and s_v , respectively.

$$s_h = (x_i - x_0) \cdot \cos \theta + (y_i - y_0) \cdot \sin \theta \quad (4)$$

$$s_v = -(x_i - x_0) \cdot \sin \theta + (y_i - y_0) \cdot \cos \theta \quad (5)$$

The coordinates of the wall reference point (x_{iw}, y_{iw}) are defined as follows

$$x_{iw} = x_0 + s_h \cdot \cos \theta \quad (6)$$

$$y_{iw} = y_0 + s_h \cdot \sin \theta \quad (7)$$

The contact is detected if

$$0 \leq s_h \leq L \text{ and } 0 \leq |s_v| \leq R_i \quad (8)$$

where

$$\sin \alpha = \frac{-(y_i - y_{iw})}{|s_v|}, \cos \alpha = \frac{-(x_i - x_{iw})}{|s_v|}, \text{gap} = |s_v| \quad (9)$$

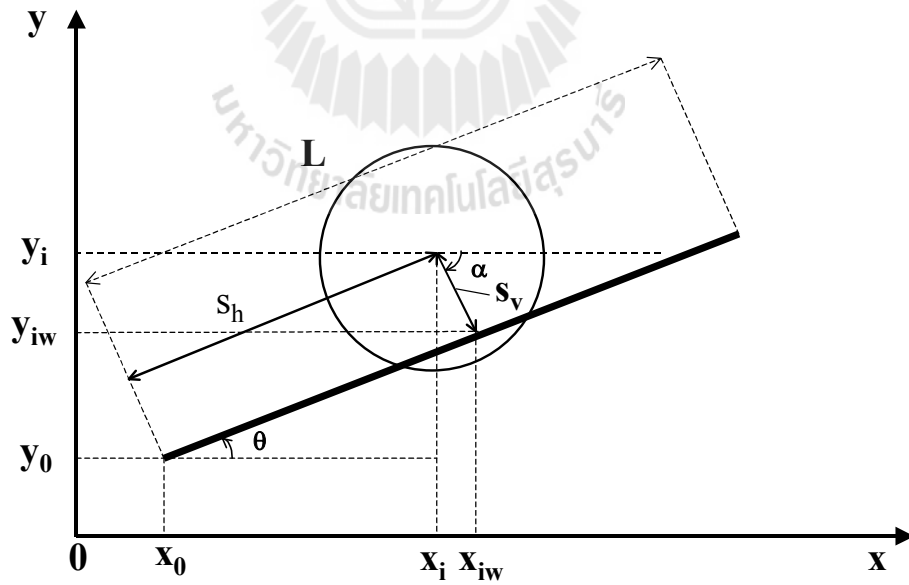


Figure 4. Contact of a particle with wall

Figure 5 illustrates the derivation of Eqs. (4) and (5).

$$1 = (y_i - y_0) \cdot \cos \theta; \quad 2 = (x_i - x_0) \cdot \sin \theta$$

$$3 = (x_i - x_0) \cdot \cos \theta; \quad 4 = (y_i - y_0) \cdot \sin \theta$$

Then, the distances s_v and s_h are formulated as

$$s_v = 1 - 2 = (y_i - y_0) \cdot \cos \theta - (x_i - x_0) \cdot \sin \theta$$

$$s_h = 3 + 4 = (x_i - x_0) \cdot \cos \theta + (y_i - y_0) \cdot \sin \theta$$

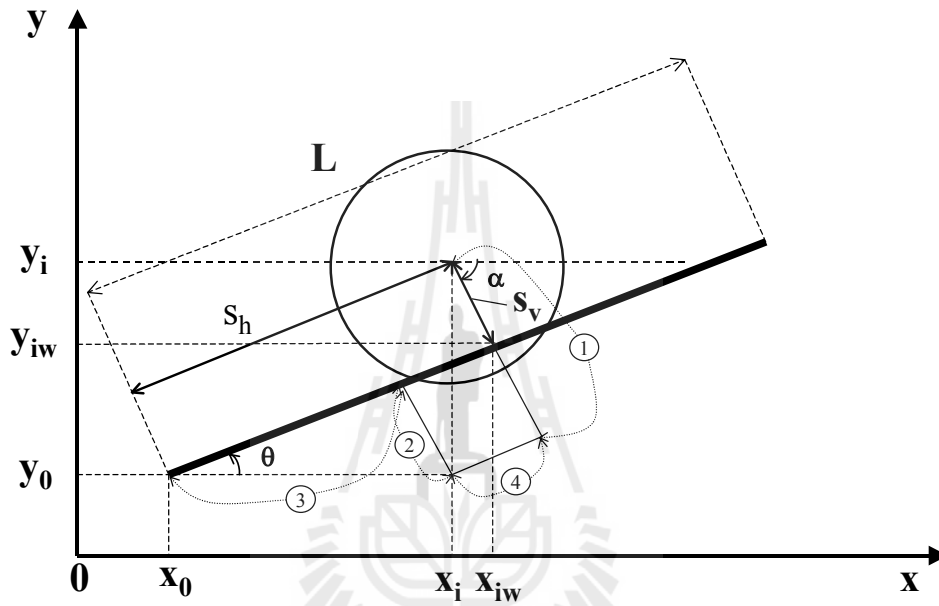


Figure 5. Derivation of particle-wall contact

2.1.3 Force balances

The linear and angular velocities of the i^{th} particle are calculated by solution of Eqs. (10) and (11). These equations are derived based on the Newton's law (Garg et al., 2011).

$$m_i \cdot \frac{d\mathbf{V}_i}{dt} = m_i \cdot \mathbf{g} + \mathbf{F}c_i \quad (10)$$

$$I_i \frac{d\omega_i}{dt} = \mathbf{T}_i \quad (11)$$

where m_i is the mass, $m_i = \frac{4\pi r_i^3}{3} \cdot \rho_i$, ρ_i is the density, V_i is the linear velocity, ω_i is the angular velocity, g is the acceleration due to the gravity, F_{c_i} is the net force exerted on the i^{th} particle by contacting particles, I_i is the moment of inertia and T_i is the sum of all torques acting on i^{th} particle.

The particle position is calculated by integration of the following equation

$$\frac{d\mathbf{X}_i}{dt} = \mathbf{V}_i \quad (12)$$

2.1.4 Contact forces

The soft-sphere model is utilized for calculation of contact forces between particles, and particles and walls (Cundall and Strack, 1979). The combination of the spring and dashpot is used both in normal and tangential directions. The dashpot accounts for the dissipation of kinetic energy during collision and the spring is used for separation of overlapping particles.

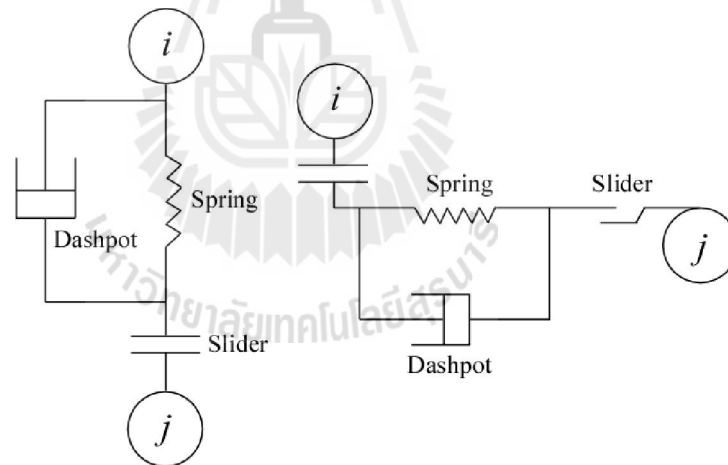


Figure 6. Illustration of dashpot-slider model

Forces acting between two particles are separated into the normal and tangential components. The normal component of the contact force is resolved into the spring and dashpot forces

$$\mathbf{F}n_{ij} = \mathbf{F}n_{ij}^S + \mathbf{F}n_{ij}^D \quad (13)$$

where $\mathbf{F}n_{ij}^S$ is the normal spring force and $\mathbf{F}n_{ij}^D$ is the normal dashpot force.

The nonlinear force-displacement relation based on the Hertzian contact theory is used for calculation of the normal stiffness of an elastic spring at the contact point between particles i and j (Kruggel-Emden et al., 2007).

The normal spring force is defined as

$$\mathbf{F}n_{ij}^S = -k_n \delta_n^{3/2} \boldsymbol{\eta}_{ij} \quad (14)$$

where k_n is the spring stiffness coefficient in the normal direction, δ_n is the overlap between particles and $\boldsymbol{\eta}_{ij}$ is the unit vector.

The normal unit vector points from the center of mass of particle j to i

$$\boldsymbol{\eta}_{ij} = \frac{\mathbf{X}_j - \mathbf{X}_i}{|\mathbf{X}_j - \mathbf{X}_i|} \quad (15)$$

The overlap of particles during the contact is

$$\delta_n = (r_i + r_j) - |\mathbf{X}_i - \mathbf{X}_j| \quad (16)$$

The spring stiffness K_n depends on the geometry and the elastic properties of contacting particles

$$K_n = \frac{4}{3} E_{eff} \sqrt{R_{eff}} \quad (17)$$

where the reduced radius R_{eff} is given by

$$R_{eff} = \left(\frac{1}{r_i} + \frac{1}{r_j} \right)^{-1} \quad (18)$$

and the effective Young's modulus E_{eff} is

$$E_{eff} = \left(\frac{1-\nu_i^2}{E_i} + \frac{1-\nu_j^2}{E_j} \right)^{-1} \quad (19)$$

Here, E_i and ν_i are the Young's modulus and Poisson ratio of i^{th} particle, respectively.

The damping dashpot force $\mathbf{F}n_{ij}^D$ is given by (EDEM, 2013)

$$\mathbf{F}n_{ij}^D = -2\sqrt{\frac{5}{6}}\beta\sqrt{S_n m_{eff}}\mathbf{V}n_{ij} \quad (20)$$

where

$$m_{eff} = \left(\frac{1}{m_i} + \frac{1}{m_j} \right)^{-1}, \quad (21)$$

$\mathbf{V}n_{ij}$ is the normal component of the relative contact velocity, and β and S_n are defined as

$$\beta = \frac{\ln e}{\sqrt{\ln^2 e + \pi^2}} \quad (22)$$

$$S_n = 2E_{ref}\sqrt{R_{ref}\delta_n} \quad (23)$$

Here, e is the coefficient of restitution.

The normal component of contact velocity is calculated from the relative velocity of particles projected in the direction of the normal unit vector.

$$\mathbf{V}n_{ij} = \mathbf{V}_{ij} \cdot \boldsymbol{\eta}_{ij} \boldsymbol{\eta}_{ij} \equiv (\mathbf{V}_i - \mathbf{V}_j) \cdot \boldsymbol{\eta}_{ij} \boldsymbol{\eta}_{ij}, \quad (24)$$

Here, \mathbf{V}_{ij} is the relative velocity of the contact point defined as

$$\mathbf{V}_{ij} = \mathbf{V}_i - \mathbf{V}_j + (L_i \boldsymbol{\omega}_i + L_j \boldsymbol{\omega}_j) \times \boldsymbol{\eta}_{ij}, \quad (25)$$

and the distances from the center of particles i and j to the contact point are given as

$$L_i = \frac{|\mathbf{X}_j - \mathbf{X}_i|^2 + r_i^2 - r_j^2}{2|\mathbf{X}_j - \mathbf{X}_i|}, L_j = |\mathbf{X}_j - \mathbf{X}_i| - L_i \quad (26)$$

The tangential component of the contact force is also decomposed into the spring and dashpot forces

$$\mathbf{F}t_{ij} = \mathbf{F}t_{ij}^S + \mathbf{F}t_{ij}^D \quad (27)$$

The tangential spring force is given by

$$\mathbf{F}t_{ij}^S = -k_t \boldsymbol{\delta}_t \quad (28)$$

where k_t is the spring stiffness coefficient in the tangential direction, $\boldsymbol{\delta}_t$ is the tangential displacement.

The spring stiffness coefficient in the tangential direction is given by

$$k_t = 8G_{ref} \sqrt{R_{ref} \delta_n} \quad (29)$$

where G_{ref} is the effective shear modulus.

At the beginning of contact, the tangential displacement δ_t is given as

$$\delta_t = \mathbf{Vt}_{ij} \cdot \min \left(\frac{|\delta_n|}{\mathbf{V}_{ij} \cdot \boldsymbol{\eta}_{ij}}, \Delta t \right) \quad (30)$$

and at time $t + \Delta t$

$$\delta_t(t + \Delta t) = \delta_t(t) + \mathbf{Vt}_{ij} \cdot \Delta t \quad (31)$$

The tangential component of contact velocity is

$$\mathbf{Vt}_{ij} = \mathbf{V}_{ij} - \mathbf{V}_{ij} \cdot \boldsymbol{\eta}_{ij} \boldsymbol{\eta}_{ij} \quad (32)$$

The sliding is taking into account if

$$|\mathbf{Ft}_{ij}| > \mu |\mathbf{Fn}_{ij}|, \quad (33)$$

and the tangential force is given by

$$\mathbf{Ft}_{ij} = \begin{cases} -\mu |\mathbf{Fn}_{ij}| \mathbf{t}_{ij} & \text{if } \mathbf{t}_{ij} \neq 0 \\ -\mu |\mathbf{Fn}_{ij}| \frac{\delta_t}{|\delta_t|} & \text{if } \mathbf{t}_{ij} = 0, \delta_t \neq 0 \\ 0 & \text{otherwise} \end{cases} \quad (34)$$

where μ is the friction coefficient.

The rolling is taken into account by using a torque on the contacting surfaces

$$\tau_i = -\mu_r \mathbf{Fn}_{ij} L_i \boldsymbol{\omega}_i \quad (35)$$

where μ_r is the coefficient of rolling friction.

The damping dashpot force \mathbf{Ft}_{ij}^D is given by

$$\mathbf{Ft}_{ij}^D = -2 \sqrt{\frac{5}{6}} \beta \sqrt{S_t m_{eff}} \mathbf{Vt}_{ij} \quad (36)$$

The total contact force on the i^{th} particle is calculated as

$$\mathbf{Fc}_i = \sum_{j=1, j \neq i}^N (F_{ij}^S + F_{ij}^D) \quad (37)$$

and the total torque acting on i^{th} particle is given by

$$\mathbf{T}_i = \sum_{j=1, j \neq i}^N \left(L_i \boldsymbol{\eta}_{ij} \times \mathbf{Ft}_{ij} \right) \quad (38)$$

2.2 Theoretical background of screening layer model

2.2.1 Outline of screening layer model

At the present study, the segregation behavior of the binary particle mixture was investigated during heap formation in filling two- and three dimensional vessels. In the three-dimensional case, the heap is formed freely inside the conical hopper and the movement of particles expands in circumferential direction during descending over inclined heap surface. However, in the two-dimensional apparatus, the particle movement is restricted in the space bounded by the parallel vertical side walls, and thus particles descend only in downward direction.

The percolation phenomena of small particles through the packed bed of larger particles were studied experimentally (Bridgwater, 1969; Shinohara et al, 1970; Fan et al., 2012) and also using the computational modeling techniques (Shinohara et al, 1972; Makse et al, 1997; Li et al, 2005; Gray, 2010; Rahman et al, 2011). The penetration rate of small particles moving through a layer of randomly packed larger particles was found to be dependent on many factors such as the size and density ratios, dynamic and static coefficients of friction, coefficients of restitution of penetrating and packing particles, local voidage of packed layer etc. (Bridgwater and Ingram, 1971; Fan et al., 2012). However, until now, there is no well-established and verified theory to predict quantitatively the extent of segregation of powder mixture by analyzing the physical interaction among particles including the elementary micro events such as collisions and rolling of separate particles over stationary particles forming the rough heap surface (Prigozin, 1993). The majority of computational models used in simulation of particle segregation in industrial processes include adjustable parameters to be fitted to specific experimental data.

The dominant segregation during heap formation is quantitatively described by adopting the screening layer model (Shinohara et al., 1972). In this model, the layer of particles formed at the heap center is assumed to be separated on sub-layers during moving along the heap as particles of smaller size separate from the mixture to the bottom of the flowing layer by penetration through the void spaces dynamically formed among the large framing particles. Therefore, a segregating sub-layer comprising the particle mixture is gradually depleted with small particles that generate

a separated lower sub-layer. At the same time, large particles make a remained upper sub-layer. Some portion of small particles in the separated layer deposit in the void space among stationary framing particles on the heap surface during flowing to form a so-called packed static sub-layer. Figure 7 illustrates the screening layer model. This model was verified by comparison of numerical results with experimental data in two-dimensional (Shinohara *et al.*, 1972) and three-dimensional (Shinohara and Enstad, 1990; Rahman *et al.*, 2011) cases.

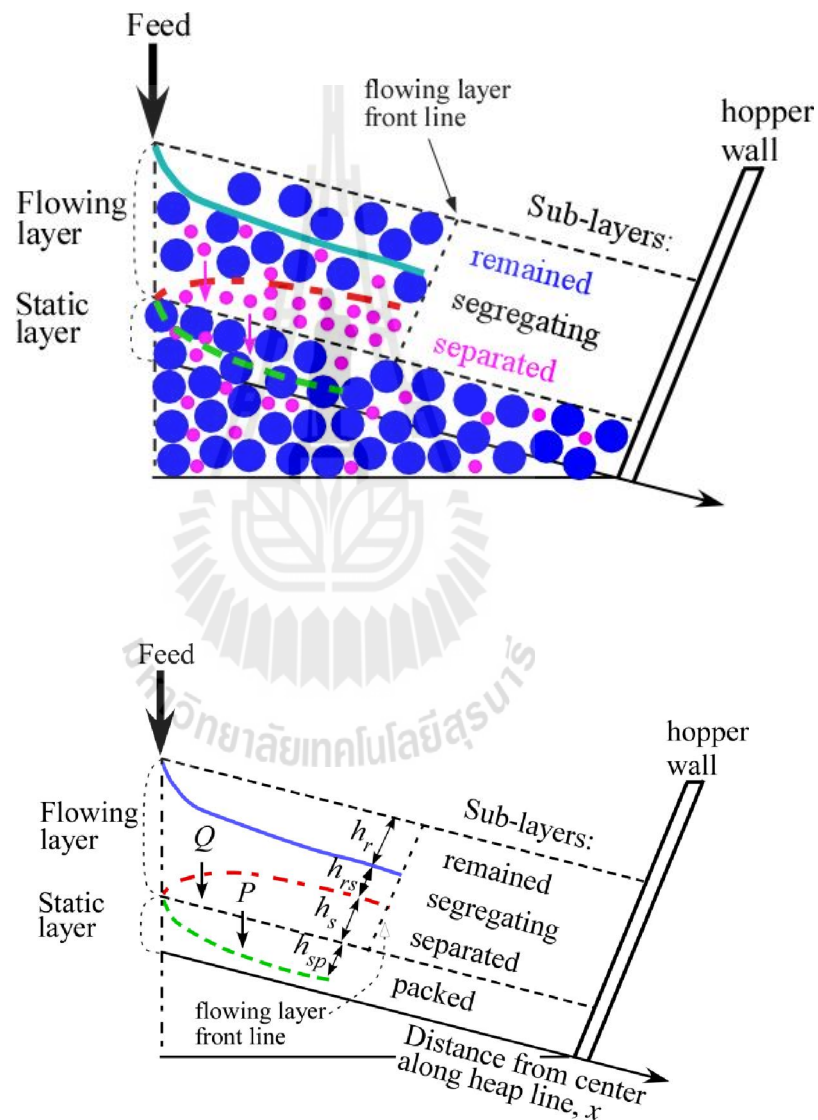


Figure 7. Illustration of screening layer model

2.2.2 Derivation of balance equations in two dimensions

To illustrate the derivation of balance equations, consider the differential element of height h_r , length Δx and thickness w in the remained flowing sub-layer. The volumetric balance over the differential element can be derived in the two-dimensional case as follows:

- Supply of particles at position x during the time interval Δt

$$h_r \cdot w \cdot v_r \Big|_x \cdot \Delta t$$

- Withdrawal of particles at position $x + \Delta x$ during the time interval Δt

$$h_r \cdot w \cdot v_r \Big|_{x+\Delta x} \cdot \Delta t$$

- Bulk volume of remaining particles derived from the segregating layer

$$V_R$$

- Accumulation of remaining particles in differential zone

$$\left(h_r \Big|_{t+\Delta t} - h_r \Big|_t \right) \cdot w \cdot \Delta x$$

The balance equation is

$$h_r \cdot w \cdot v_r \Big|_x \cdot \Delta t - h_r \cdot w \cdot v_r \Big|_{x+\Delta x} \cdot \Delta t + V_R = \left(h_r \Big|_{t+\Delta t} - h_r \Big|_t \right) \cdot w \cdot \Delta x \quad (39)$$

where h_r is the thickness of remained sub-layer, v_r is the sub-layer velocity, x is the distance from the center along the heap line, t is the time and w is the sub-layer depth.

Dividing by $w \cdot \Delta x \cdot \Delta t$ and taking limits at $\Delta t \rightarrow 0$ and $\Delta x \rightarrow 0$ results in a partial differential equation for remained sub-layer

$$\frac{\partial h_r}{\partial t} = - \frac{\partial (h_r v_r)}{\partial x} + \frac{V_R}{\Delta x \cdot w \cdot \Delta t} \quad (40)$$

The volumetric balance over the differential zone of the intermediate segregating sub-layer is

$$\frac{\partial h_{rs}}{\partial t} = - \frac{\partial (h_{rs} v_{rs})}{\partial x} - \frac{V_R + V_S}{\Delta x \cdot w \cdot \Delta t} \quad (41)$$

where h_{rs} and v_{rs} are the thickness and velocity of segregating sub-layer, respectively. Here, V_s is the bulk volume of separated particles derived from the segregating sub-layer and delivered to the separated one.

The volumetric balance of the separated sub-layer is

$$\frac{\partial h_s}{\partial t} = -\frac{\partial(h_s v_s)}{\partial x} + \frac{V_s - V_p}{\Delta x \cdot w \cdot \Delta t} \quad (42)$$

where h_s and v_s are the thickness and velocity of separated sub-layer, respectively. Here, V_p is the bulk volume of separated particles derived from the separated sub-layer and delivered to the packed one.

The volumetric balance for packed static sub-layer is

$$\frac{\partial h_{sp}}{\partial t} = \frac{V_p}{\Delta x \cdot w \cdot \Delta t} \quad (43)$$

The penetration rate of separated particles is related to V_s as

$$Q = \frac{V_s \cdot (1 - \varepsilon)}{\Delta x \cdot w \cdot \Delta t \cdot \cos \phi} \quad (44)$$

where Q is the penetration rate of separated particles through the unit overall area of the segregating layer on the net volume basis, i.e. the penetrating flux, ε is the sub-layer voidage and ϕ is the pouring angle of repose.

The packing rate P is related to V_p as

$$V_p = \frac{P \cdot \Delta x \cdot w \cdot \Delta t \cdot \cos \phi}{1 - \varepsilon} \quad (45)$$

The relation between V_R and V_s is

$$V_R = V_s \cdot \left(\frac{1 - M_i}{M_i} \right) \quad (46)$$

where M_i is the initial mixing ratio of segregating component.

Using Eqs. (44) - (46), the balance Eqs. (40) - (43) can be rewritten as

- Upper remained sub-layer:

$$\frac{\partial h_r}{\partial t} = -\frac{\partial(h_r v_r)}{\partial x} + \frac{Q \cos \phi}{(1 - \varepsilon_r)} \cdot \frac{1 - M_i}{M_i} \quad (47)$$

- Intermediate segregating sub-layer:

$$\frac{\partial h_{rs}}{\partial t} = -\frac{\partial(h_{rs}v_{rs})}{\partial x} - \frac{Q\cos\phi}{M_i(1-\varepsilon_{rs})} \quad (48)$$

- Lower separated sub-layer:

$$\frac{\partial h_s}{\partial t} = -\frac{\partial(h_s v_s)}{\partial x} + \frac{(Q-P)\cos\phi}{(1-\varepsilon_s)} \quad (49)$$

- Static packed sub-layer:

$$\frac{\partial h_{sp}}{\partial t} = \frac{P\cos\phi}{(1-\varepsilon_{sp})} \quad (50)$$

The total thickness of the flowing layer, $h_t = h_r(t, x) + h_{rs}(t, x) + h_s(t, x)$, and the velocity ratio of the lower separated sub-layer to the upper remained one, $R = v_s(t, x)/v_r(t, x)$, are assumed to be constant.

$$h_t = h_r(t, x) + h_{rs}(t, x) + h_s(t, x) = \text{const} \quad (51)$$

The velocity of remained sub-layer, $v_r(t, x)$, is supposed to be equal to that of segregating sub-layer, $v_{rs}(t, x)$.

$$v_r(t, x) = v_{rs}(t, x) \quad (52)$$

Finally, the balance equations for the flowing layer can be summarized in two-dimensional case as

- Upper remained sub-layer:

$$\frac{\partial h_r}{\partial t} = -\frac{\partial(h_r v_r)}{\partial x} + \frac{Q\cos\phi}{(1-\varepsilon_r)} \cdot \frac{1-M_i}{M_i} \quad (53)$$

- Intermediate segregating sub-layer:

$$\frac{\partial h_{rs}}{\partial t} = -\frac{\partial(h_{rs} v_r)}{\partial x} - \frac{Q\cos\phi}{M_i(1-\varepsilon_{rs})} \quad (54)$$

- Lower separated sub-layer:

$$\frac{\partial h_s}{\partial t} = -\frac{\partial(h_s R v_r)}{\partial x} + \frac{(Q-P)\cos\phi}{(1-\varepsilon_s)} \quad (55)$$

2.2.3 Velocity of flowing sub-layers

As the total thickness does not change with time, the following equations can be written

$$\frac{\partial h_t}{\partial t} = \frac{\partial (h_r + h_{rs} + h_s)}{\partial t} = 0 \quad (56)$$

Substitution of right-hand sides of Eqs. (47) - (49) into Eq. (56) yields

$$\frac{\partial (h_r v_r)}{\partial x} + \frac{\partial (h_{rs} v_{rs})}{\partial x} + \frac{\partial (h_s v_s)}{\partial x} = \frac{Q \cos \phi}{1 - \varepsilon_r} \cdot \frac{1 - M_i}{M_i} - \frac{Q \cdot \cos \phi}{M_i (1 - \varepsilon_{rs})} + \frac{(Q - P) \cos \phi}{(1 - \varepsilon_s)} \quad (57)$$

Using Eq. (52), Eq. (57) could be simplified as

$$\frac{\partial (h_r v_r)}{\partial x} + \frac{\partial (h_{rs} v_r)}{\partial x} + \frac{\partial (h_s R v_r)}{\partial x} = \frac{Q \cos \phi}{1 - \varepsilon_r} \cdot \frac{1 - M_i}{M_i} - \frac{Q \cdot \cos \phi}{M_i (1 - \varepsilon_{rs})} + \frac{(Q - P) \cos \phi}{(1 - \varepsilon_s)} \quad (58)$$

The thickness of remained sub-layer is evaluated from the total thickness of the flowing layer as $h_r(t, x) = h_t - h_{rs}(t, x) - h_s(t, x)$. The left-hand side of Eq. (58) become

$$\frac{\partial (h_r v_r)}{\partial x} + \frac{\partial (h_{rs} v_r)}{\partial x} + \frac{\partial (h_s R v_r)}{\partial x} = \frac{\partial (h_r + h_{rs} + h_s R) v_r}{\partial x} = \frac{\partial (h_t - h_s + h_s R) v_r}{\partial x}$$

Equation (58) can be rearranged as

$$\frac{\partial (h_t - h_s (1 - R)) \cdot v_r}{\partial x} = \frac{Q \cdot \cos \phi}{M_i} \left(\frac{1 - M_i}{1 - \varepsilon_r} - \frac{1}{1 - \varepsilon_{rs}} \right) + \frac{(Q - P) \cdot \cos \phi}{(1 - \varepsilon_s)} \quad (59)$$

Using the product rule of differentiation, the left-hand side of Eq. (59) can be expanded as

$$(h_t - h_s (1 - R)) \cdot \frac{\partial v_r}{\partial x} - (1 - R) v_r \cdot \frac{\partial h_s}{\partial x} = \frac{Q \cdot \cos \phi}{M_i} \left(\frac{1 - M_i}{1 - \varepsilon_r} - \frac{1}{1 - \varepsilon_{rs}} \right) + \frac{(Q - P) \cdot \cos \phi}{(1 - \varepsilon_s)}$$

Finally, the variation of velocity along the distance x is

$$\frac{\partial v_r}{\partial x} = \frac{(1 - R) v_r}{h_t - h_s (1 - R)} \cdot \frac{\partial h_s}{\partial x} + \frac{Q \cdot \cos \phi}{M_i \cdot (h_t - h_s (1 - R))} \left(\frac{1 - M_i}{1 - \varepsilon_r} - \frac{1}{1 - \varepsilon_{rs}} \right) + \frac{(Q - P) \cdot \cos \phi}{(1 - \varepsilon_s) \cdot (h_t - h_s (1 - R))} \quad (60)$$

2.2.4 Penetration rate

The penetration rate of segregating particles is considered to be the product of the number of discharge openings among large framing particles per unit cross-sectional area and the volumetric flow rate of the penetrating small particles through each openings (Shinohara et al., 1972).

The number of discharge openings per unit cross-sectional area is

$$\delta \cdot \frac{1 - \varepsilon_f}{\pi d_f^2} \quad (61)$$

where δ is the number of effective openings per number of framing particles,

$\frac{1 - \varepsilon_f}{\pi d_f^2 / 6}$ is the number of framing particles per unit cross-sectional area.

The volumetric flow rate of penetrating particles is

$$\alpha \cdot (D_e - d_s)^p \quad (62)$$

where D_e is the equivalent opening diameter of the effective void spaces among the framing particles, d_s is the diameter of segregating particles, and α and p are constants.

Thus, the penetration rate is

$$Q = \delta \cdot \frac{1 - \varepsilon_f}{\pi d_f^2 / 6} \cdot \alpha \cdot (D_e - d_s)^p \quad (63)$$

The total effective area of the screen openings is

$$S \cdot \varepsilon_f (1 - \beta)$$

where S is the cross-sectional area and β is the fraction of ineffective area for separation in the voids.

The total effective area can be calculated as the product of the area of one screen opening and the number of discharge openings among framing particles. The area of one screen opening is $\frac{\pi D_e^2}{4}$ and the number of discharge openings among framing

particles is $\delta \cdot \frac{1 - \varepsilon_f}{\pi d_f^2 / 6} \cdot S$.

Combining all terms yields

$$S \cdot \varepsilon_f (1 - \beta) = \left(\frac{\pi D_e^2}{4} \right) \cdot \left(\delta \cdot \frac{1 - \varepsilon_f}{\pi d_f^2 / 6} \right) \cdot S$$

The equivalent opening diameter of the void spaces is obtained by rearrangement of above equation

$$D_e = d_f \cdot \sqrt{\frac{2}{3} \cdot \frac{1-\beta}{\delta}} \cdot \sqrt{\frac{\varepsilon_f}{1-\varepsilon_f}} \quad (64)$$

Substitution of Eq. (64) into Eq. (63) results in

$$Q = \delta \cdot \frac{1-\varepsilon_f}{\pi d_f^2 / 6} \cdot \alpha \cdot \left(d_f \sqrt{\frac{2(1-\beta)}{3\delta}} \cdot \sqrt{\frac{\varepsilon_f}{1-\varepsilon_f}} - d_s \right)^p \quad (65)$$

Using constants $A = \alpha \cdot \delta$ and $B = \sqrt{\frac{2(1-\beta)}{3\delta}}$, Eq. (65) can be rewritten as

$$Q = A \cdot \frac{1-\varepsilon_f}{\pi d_f^2 / 6} \cdot \left(B \cdot d_f \cdot \sqrt{\frac{\varepsilon_f}{1-\varepsilon_f}} - d_s \right)^p \quad (66)$$

The overall void fraction ε is defined as

$$\varepsilon = \varepsilon_f (1-\beta) \varepsilon_s + \beta \cdot \varepsilon_s \quad (67)$$

where ε_s is the voidage of segregating small particles and ε_f is voidage of framing particles.

The mixing ratio M_i of segregating component is

$$M_i = \frac{\varepsilon_f (1-\beta)(1-\varepsilon_s)}{(1-\varepsilon_s) + \varepsilon_f (1-\beta)(1-\varepsilon_s)} \quad (68)$$

Substituting Eq. (67) into Eq. (68) results in

$$M_i = \frac{\varepsilon_f - \varepsilon}{1 - \varepsilon} \quad (69)$$

Finally, the voidage of framing particles is expressed as

$$\varepsilon_f = (1 - \varepsilon) M_i + \varepsilon \quad (70)$$

Using Eq. (70), Eq. (66) could be written as

$$Q = A \cdot \frac{(1-\varepsilon)(1-M_i)}{\pi d_f^2 / 6} \cdot \left(B \cdot d_f \cdot \sqrt{\frac{(1-\varepsilon)M + \varepsilon}{(1-\varepsilon)(1-M)}} - d_s \right)^p \quad (71)$$

The net volumetric feed rate F_V is defined using the total thickness of flowing sub-layers h_t and the average velocity v_{av} as

$$F_V = v_{av} \cdot h_t \cdot w \cdot (1 - \varepsilon) \quad (72)$$

The overall void fraction ε is expressed by rearrangement of Eq. (72) as

$$\varepsilon = 1 - \frac{F_V}{v_{av} \cdot h_t \cdot w} \quad (73)$$

Introducing the parameter K ,

$$K = v_{av} \cdot h_t \cdot w = \frac{F_V}{1 - \varepsilon}, \quad (74)$$

the term $\sqrt{\frac{(1-\varepsilon)M_i + \varepsilon}{(1-\varepsilon)(1-M_i)}}$ can be rearranged as

$$\begin{aligned} \sqrt{\frac{(1-\varepsilon)M_i + \varepsilon}{(1-\varepsilon)(1-M_i)}} &= \sqrt{\frac{M_i + \varepsilon(1-M_i)}{(1-\varepsilon)(1-M_i)}} = \sqrt{\frac{M_i + (1-M_i)\left(1 - \frac{F_V}{v_{av} \cdot h_t \cdot w}\right)}{(1-M_i)\frac{F_V}{v_{av} \cdot h_t \cdot w}}} = \\ &= \sqrt{\frac{1 - (1-M_i)\frac{F_V}{v_{av} \cdot h_t \cdot w}}{(1-M_i)\frac{F_V}{v_{av} \cdot h_t \cdot w}}} = \sqrt{\frac{v_{av} \cdot h_t \cdot w}{F_V(1-M_i)} - 1} = \sqrt{\frac{K}{F_V(1-M_i)} - 1} \end{aligned} \quad (75)$$

Substituting Eq. (73) into Eq. (71) yields

$$Q = \frac{6A}{\pi d_f^2} \cdot \frac{F_V}{v_{av} h_t w} \cdot (1-M_i) \cdot \left[B \cdot d_f \sqrt{\frac{v_{av} h_t w}{F_V(1-M_i)} - 1} - d_s \right]^p$$

and using Eq. (75)

$$Q = \frac{6}{\pi d_f^2} \cdot \frac{A}{K} \cdot (1-M_i) \cdot F_V \left[B \cdot d_f \sqrt{\frac{K}{F_V(1-M_i)} - 1} - d_s \right]^p$$

Finally, the penetration rate is derived as

$$Q = \frac{6d_f^{p-2}}{\pi} \frac{A}{K} (1-M_i) F_V \left[B \sqrt{\frac{K}{F_V(1-M_i)} - 1} - \frac{d_s}{d_f} \right]^p \quad (76)$$

Balance equations in two dimensions

The balance equations in two dimensions are summarized in the form of partial differential equations as follows:

- Upper remained sub-layer

$$\frac{\partial h_r}{\partial t} = -\frac{\partial(h_r v_r)}{\partial x} + \frac{Q \cos \phi}{(1-\varepsilon_r)} \cdot \frac{1-M_i}{M_i} \quad (77)$$

- Intermediate segregating sub-layer

$$\frac{\partial h_{rs}}{\partial t} = -\frac{\partial(h_{rs}v_r)}{\partial x} - \frac{Q\cos\phi}{M_i(1-\varepsilon_{rs})} \quad (78)$$

- Lower separated sub-layer

$$\frac{\partial h_s}{\partial t} = -R\frac{\partial(h_s v_r)}{\partial x} + \frac{(Q-P)\cos\phi}{(1-\varepsilon_s)} \quad (79)$$

- Static packed sub-layer

$$\frac{\partial h_{sp}}{\partial t} = \frac{P\cos\phi}{(1-\varepsilon_s)} \quad (80)$$

The boundary conditions at $x = 0$ for Eqs. (77)-(80) and Eq. (60) are

$$\begin{aligned} h_r(t, 0) &= h_s(t, 0) = h_{sp}(t, 0) = 0 \\ h_{rs}(t, 0) &= h_i \\ v_r(t, 0) &= v_{rs,i} \end{aligned} \quad (81)$$

where $v_{rs,i}$ is the initial velocity of segregating sub-layer.

The initial conditions at $t = 0$ for Eqs. (77)-(80) and Eq. (60) are

$$\begin{aligned} h_r(0, x) &= h_s(0, x) = h_{sp}(0, x) = h_{rs}(0, x) = 0 \\ v_r(0, x) &= 0 \end{aligned} \quad (82)$$

The volumetric mixing ratio at any distance x is given by

$$M_t(x) = \frac{h_{rs}(t, x)(1-\varepsilon_{rs})M_i + [h_s(t, x) + h_{sp}(t, x)](1-\varepsilon_s)}{h_r(t, x)(1-\varepsilon_r) + h_{rs}(t, x)(1-\varepsilon_{rs}) + [h_s(t, x) + h_{sp}(t, x)](1-\varepsilon_s)} \quad (83)$$

2.2.5 Balance equations in three dimensions

The balance equations in three dimensions are summarized in the form of partial differential equations as follows (Rahaman *et al.*, 2011):

- remained sub-layer

$$\frac{\partial h_r}{\partial t} = -\frac{\partial(h_r x v_r)}{x \partial x} + Q\cos\phi \frac{1-M_i}{M_i(1-\varepsilon_r)} \quad (84)$$

- segregating sub-layer

$$\frac{\partial h_{rs}}{\partial t} = -\frac{\partial(h_{rs} x v_r)}{x \partial x} - \frac{Q\cos\phi}{M_i(1-\varepsilon_{rs})} \quad (85)$$

- separated sub-layer

$$\frac{\partial h_s}{\partial t} = -\frac{\partial(h_s x v_s)}{x \partial x} + \frac{(Q-P)\cos\phi}{(1-\varepsilon_s)} \quad (86)$$

- packed sub-layer

$$\frac{\partial h_{sp}}{\partial t} = \frac{P \cos \phi}{(1 - \varepsilon_{sp})} \quad (87)$$

In contrast to the two-dimensional case, the velocity of each sub-layer decreases during descending along the heap to compensate for expansion of area available for flow at constant feed rate.

$$v_{av,x} = \frac{F_v}{2\pi h_i (1 - \varepsilon) \cos \phi} \quad (88)$$

The velocity of remaining sub-layer is given by the following differential equation

$$\frac{\partial \left[\{h_t - h_s (1 - R)\} v_{r,x} \right]}{\partial x} = x \left[\frac{Q \cos \phi}{M_i} \left\{ \frac{1 - M_i}{1 - \varepsilon_r} - \frac{1}{1 - \varepsilon_s} \right\} \frac{(Q - P) \cos \phi}{(1 - \varepsilon_s)} \right] \quad (89)$$

The system of partial differential equations was solved numerically using the method of lines with finite difference approximation of spatial derivatives (Schiesser and Griffiths, 2009). The resultant system of ordinary differential equations was solved using the backward difference method for stiff equations (Gear, 1971).

3. Simulation

3.1 Particle mixture definition

The particle diameter ratio is defined as

$$\phi_d = \frac{d_c}{d_f} \quad (90)$$

where d_c and d_f are the diameter of coarse and fine particles, respectively.

The initial mixing ratio of fine segregating particles is given as

$$M_i = \frac{N_f \cdot \frac{\pi d_f^3}{6} \cdot \rho_f}{N_f \cdot \frac{\pi d_f^3}{6} \cdot \rho_f + N_c \cdot \frac{\pi d_c^3}{6} \cdot \rho_c} \quad (91)$$

where N_c and N_f are the number of coarse and fine particles, and ρ_c and ρ_f are the density of coarse and fine particles, respectively.

Assuming that $\rho_c = \rho_f$, Eq. (91) can be simplified as

$$M_i = \frac{1}{1 + \frac{N_c}{N_f} \cdot \phi_d^3} \quad (92)$$

For the given initial mixing ratio M_i , the particle diameter ratio ϕ_d and the total number of particles $N_t = N_f + N_c$, the number of fine particles is calculated as

$$N_f = \frac{N_t \cdot M_i \cdot \phi_d^3}{x_f (\phi_d^3 - 1) + 1} \quad (93)$$

The target number of fine and coarse particles generated in a feed stream per unit time was chosen to satisfy both the initial mixing ratio by Eq. (92) and the required total feed rate.

3.2 Setup of discrete element simulations

The two-dimensional simulation setup was constructed to emulate an experimental system used in our previous work (Shinohara *et al.*, 2001), as shown in Fig. 8. To decrease the calculation time, only half of experimental system was simulated assuming that the system is symmetric. The simulation setup consists of two parallel

plates separated by a distance of 10 mm and a feed tank, as illustrated in Fig. 9. The feed tank moves upward to keep the distance between the feed tank outlet and the heap top approximately constant from 2 to 5 diameters of large particles. Particles are generated randomly on a virtual feed plate located inside the feed tank.

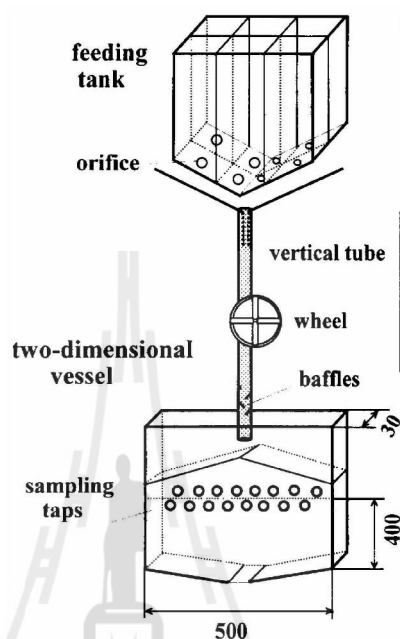


Figure 8. Experimental two-dimensional system for measuring particle segregation (Shinohara et al., 2001)

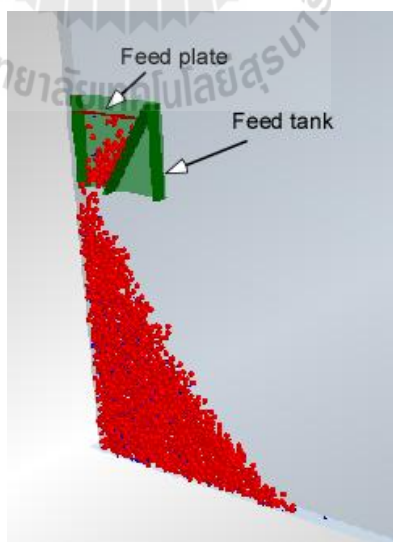


Figure 9. Two-dimensional simulation setup

The initial conditions for particle generation are summarized in Table 1.

Table 1. Initial conditions for particle generation in two-dimensional simulation

Simulation case	Initial mixing ratio, M_i	The number of fine particles per second, N_f / s	The number of coarse particles per second, N_c / s
1	0.01	202	750
2	0.1	2046	682
3	0.3	6140	531

Here, the particle size ratio and the total feed rate were kept constant as $\phi_d = 3$ and $f_t = 3.17 \text{ cm}^3/\text{s}$. The glass particles of $d_c = 2 \text{ mm}$ and $d_f = 0.67 \text{ mm}$ were used in simulation. The total number of particles was 9525 in a simulation Case 1, 27280 in Case 2 and 66710 in Case 3. The material and flow properties of particles and walls are summarized in Table 2.

Table 2. Material and flow properties of particles and walls.

Property	glass	steel
Poisson's ratio	0.25	0.28
Shear modulus, [Pa]	7e+10	2e+11
Density, [kg/m ³]	2500	7900
Coefficient of restitution	0.5	0.5
Coefficient of static friction	0.5	0.5
Coefficient of rolling friction	0.2	0.5

To analyze the segregation behavior of particles mixture during the heap formation, the slice of the heap of width 10 mm and depth of 6 mm was taken along the heap line. The distance from the heap top to the bottom was divided into 10 equal intervals and the slice was separated on ten boxes according to the interval positions, as

illustrated in Fig. 10. The concentration of fine particles M_j was calculated by counting all particles in the box.

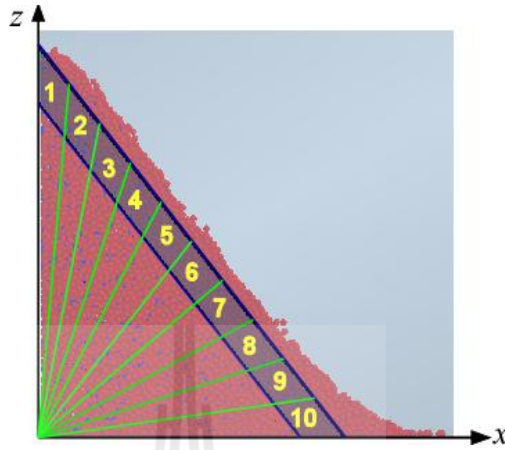


Figure 10. Illustration of measuring positions along the heap line.

The segregation index I_s is defined in terms of a coefficient of variation given by

$$I_s = \frac{\sigma}{M_i} \quad (94)$$

where σ is the deviation of mixing ratio of the segregating small component at different sampling positions along the heap line, M_j , from the initial mixing ratio, M_i :

$$\sigma^2 = \frac{1}{N_s - 1} \sum_{j=1}^{N_s} (M_j - M_i)^2 \quad (95)$$

Here, N_s is the number of sampling points.

4. Results and Discussion

4.1 Simulation results by discrete element method

4.1.1 Calibration of simulation model

The DEM simulation model was calibrated by adjusting the coefficient of rolling friction to have an angle of repose of coarse particles similar to the experimental one. Figure 11 illustrates the measuring procedure of the angle of repose. The results of simulation are shown in Fig. 12 and the results of measurement are summarized in Table 3.

As a result, the angle of repose in a heap formed using the coefficient of rolling friction of 0.2 is 29.5° which is most close to the experimentally measured angle of repose of 30° .

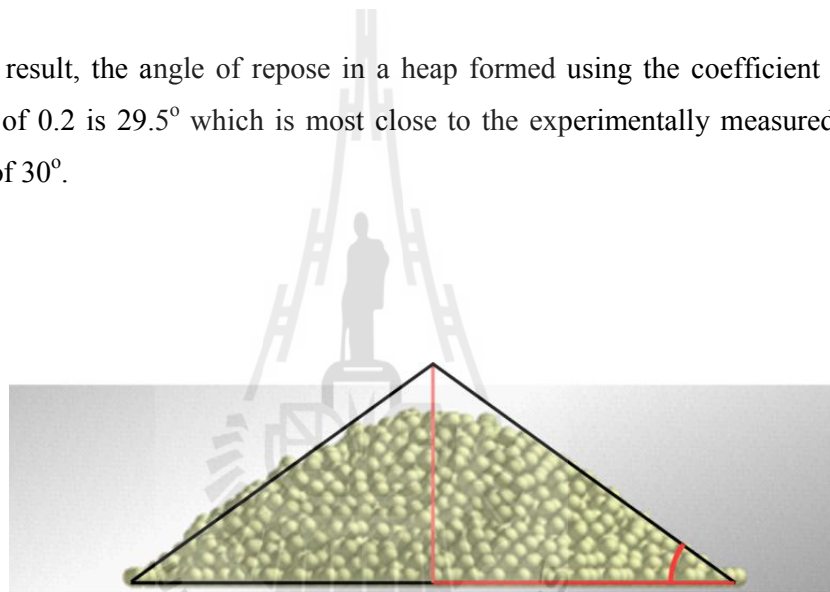


Figure 11. Illustration of measurement of angle of repose

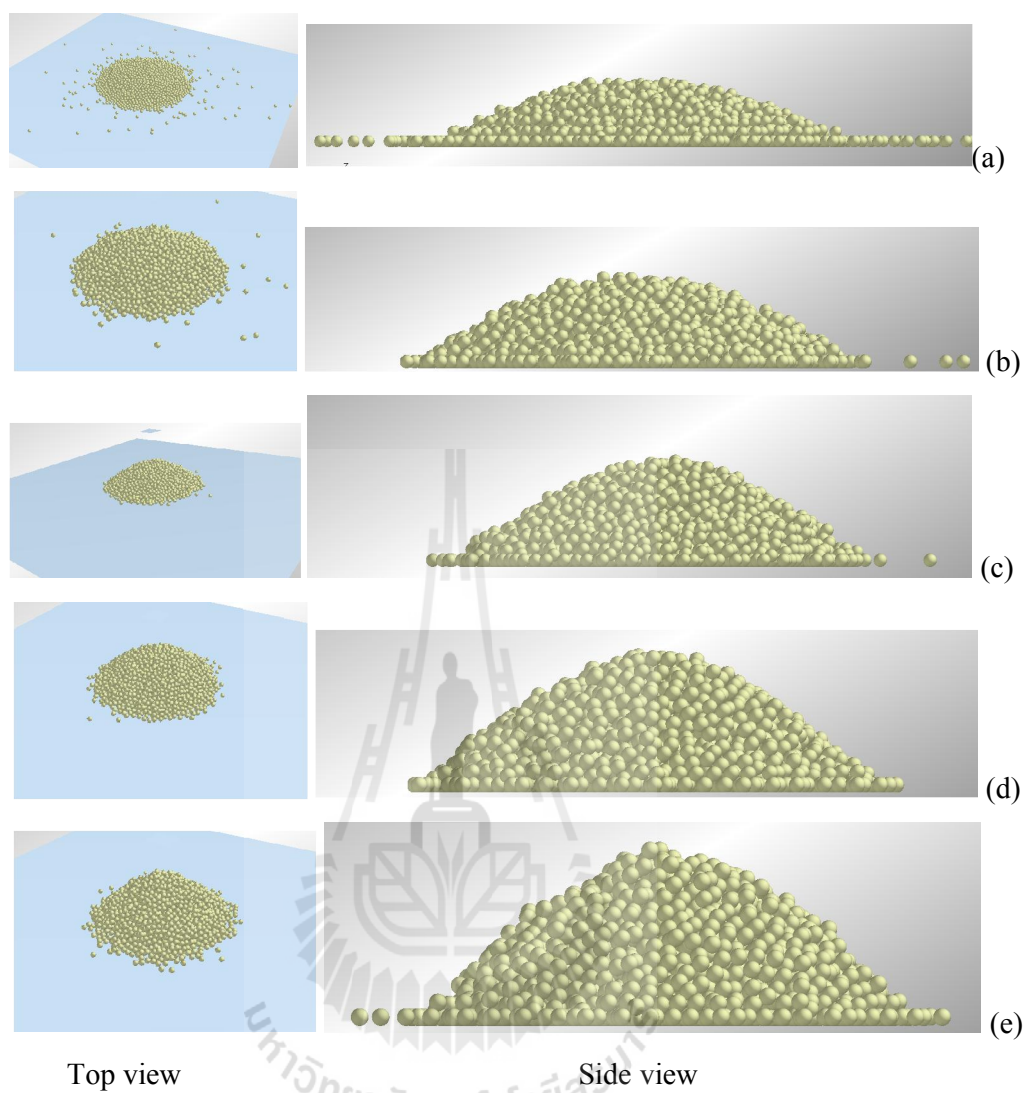
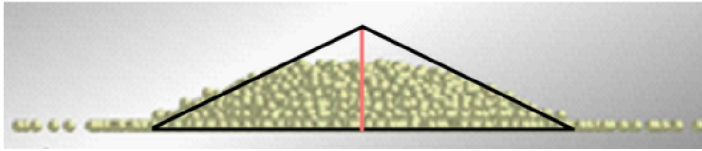
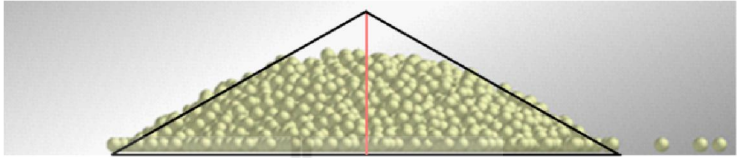
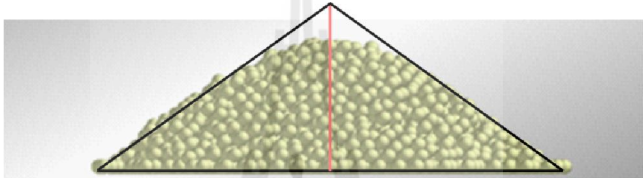
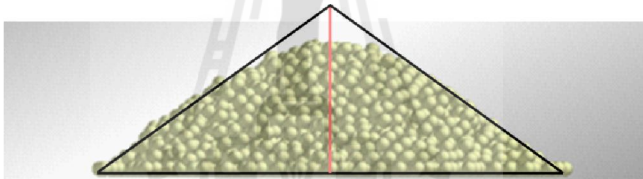
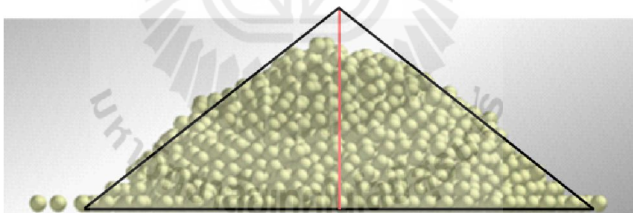


Figure 12. Effect of coefficient of rolling friction on particle heap formation:

(a) 0.1, (b) 0.2, (c) 0.3, (d) 0.4, (e) 0.5.

Table 3. Angle of repose in heap formed with various coefficients of rolling friction

Coefficient of rolling friction	Illustration of measurement of angle of repose	Angle of repose, [°]
0.1		26.5
0.2		29.5
0.3		32.4
0.4		35.9
0.5		38.3

4.1.2 Segregation simulation results by DEM

Snapshots of simulation results for various initial concentrations of fine component generated using input data in the Table 1 are shown in Figs. 13 (a), (b) and (c), respectively. These results confirm that fine particles (blue color) concentrate close to the heap center.

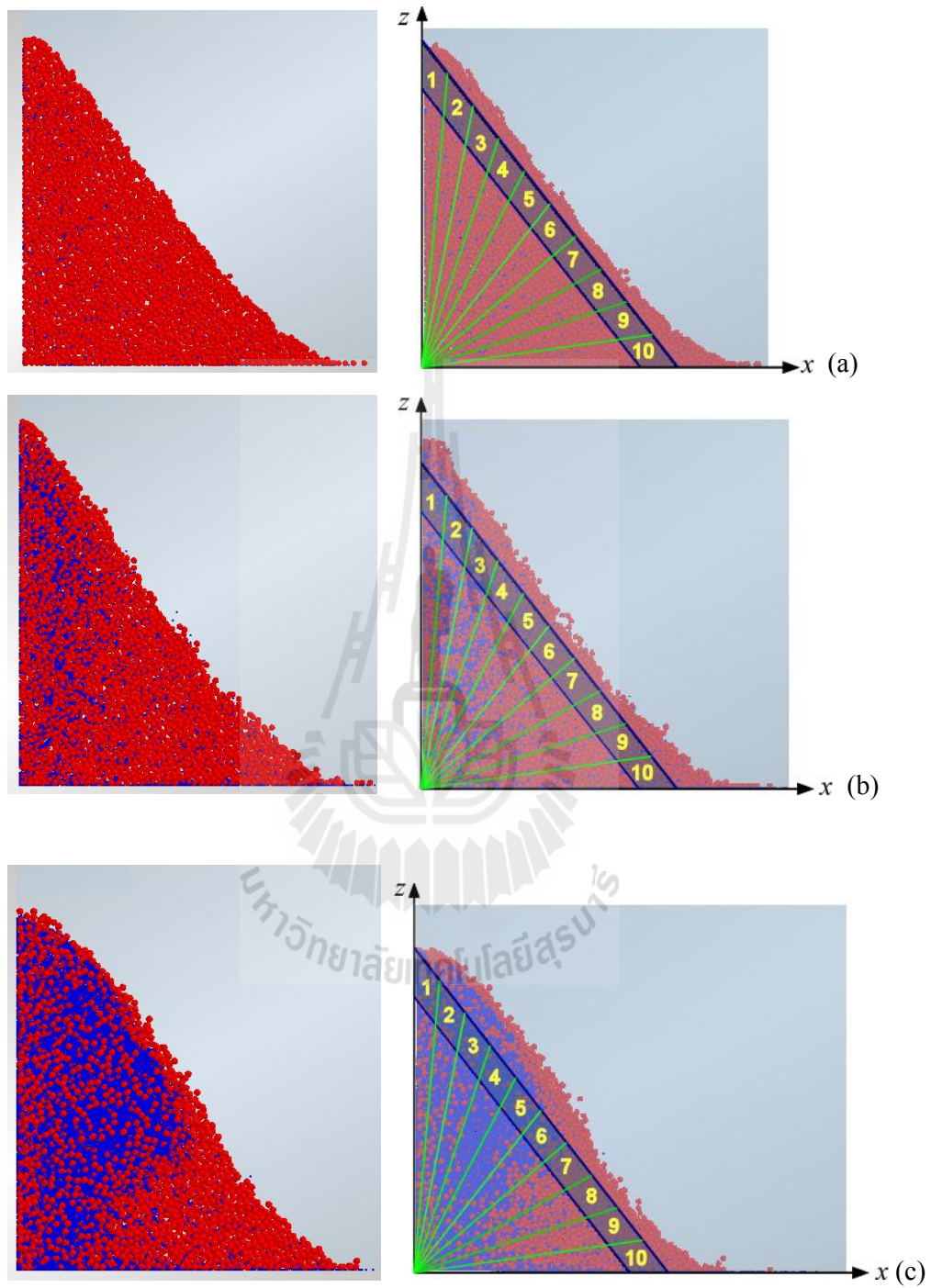


Figure 13. Snapshots of two-dimensional simulation results for various initial concentrations of fine component: (a) 0.01, (b) 0.1, (c) 0.3.

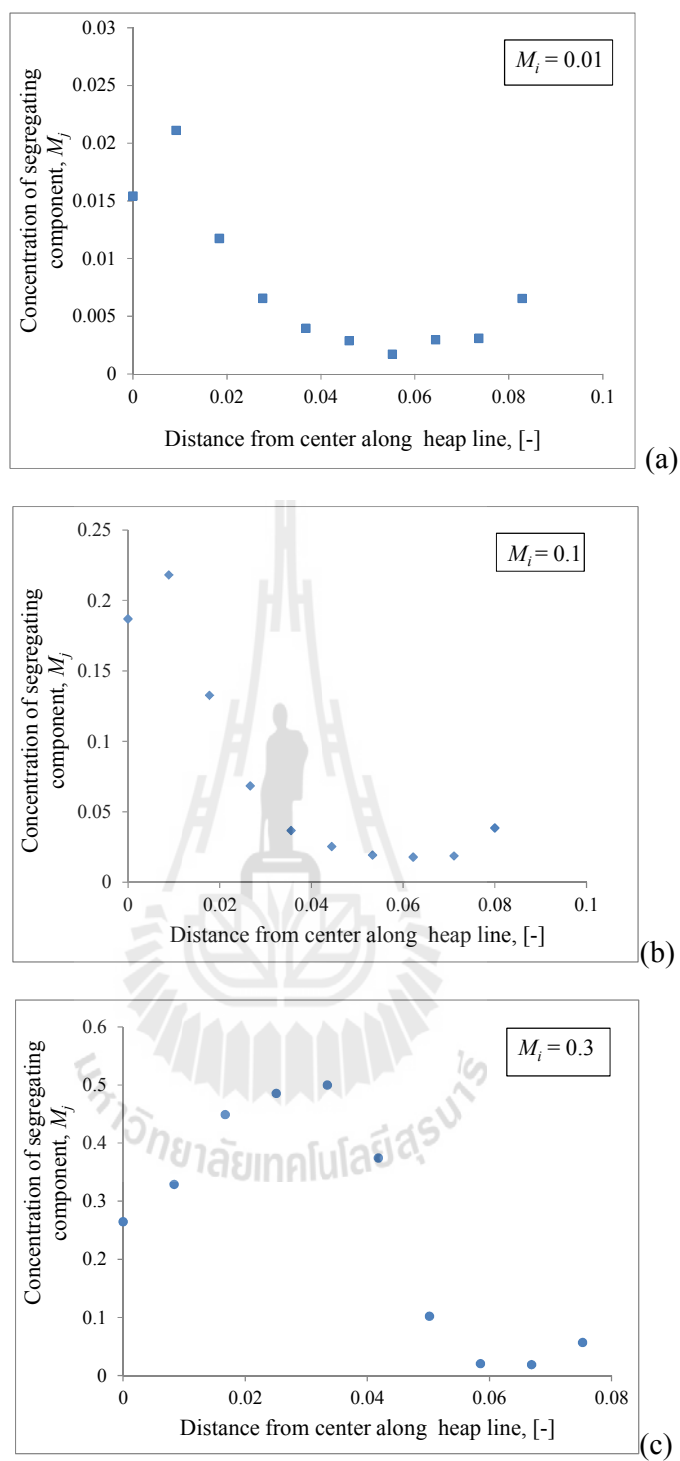


Figure 14. Distribution of segregating component along heap line:

(a) 0.01, (b) 0.1, (c) 0.3.

Figure 14 illustrate the distributions of fine component along the heap line for various initial concentrations of segregating component. The distribution profile is sharper with higher peak located close to the heap center at the lower initial concentration of fine component. This is also confirmed by higher value of segregation index at lower initial concentration as shown in Fig. 15. The fine particles are penetrated through voids among coarse particles formed during flow along the heap line. In case of small amount of fine particles, it is easy for them to separate from the main stream close to the heap center and penetrate to the lower static layer. However, in the case of large initial amount of fine particles some of them are dragged down the heap line by larger particles as voids close to the center already occupied. Segregation profiles simulated by the discrete element method are similar to ones calculated by the screening layer model (see Fig. 23) conforming the applicability of DEM models for generation of data to be used in the analysis of segregation mechanism in industrial apparatus.

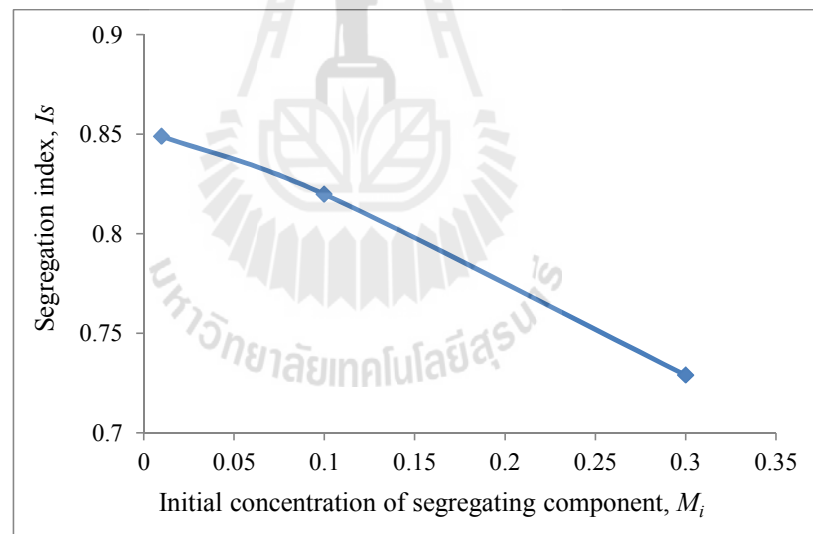


Figure 15. Variation of segregation index with initial concentration of segregating component

4.2 Calculation results by screening layer model

4.2.1 Model calibration

Figure 16 illustrates the validation of two-dimensional model by fitting experimental data with calculated curve. The parameters used in calculation by the screening layer model are summarized in Table 4.

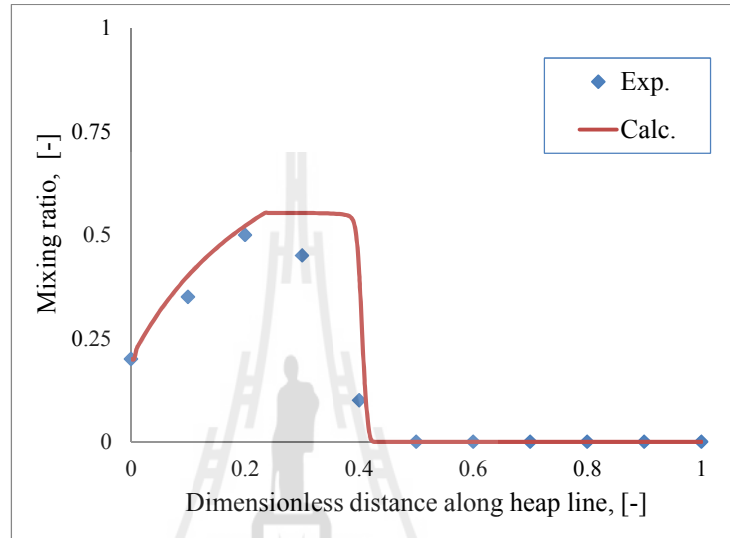


Figure 16. Validation of two-dimensional screening layer model by fitting experimental data

Table 4. Operational and flowability parameters used in 2D model validation

Parameter	Value
Initial mixing ratio of segregating component, [-]	0.2
Feed rate on net volume basis, [cm ³ /s]	42
Total thickness of flowing layer, [cm]	0.5
Length of heap line, [cm]	30
Width of apparatus, [cm]	10
Penetration rate of segregating component, [cm/s]	0.12
Velocity ratio of separated to framing components, [-]	0.2
Packing rate of segregating component, [cm/s]	0.01
Void fraction of remained sub-layer, [-]	0.2
Void fraction of segregating sub-layer, [-]	0.5
Void fraction of separated sub-layer, [-]	0.5

Figure 17 illustrates the validity of three-dimensional screening layer model by comparison of experimental data with calculated results. The parameters used in simulation are summarized in Table 5.

Figures 9 and 10 confirm the validity of two and three dimensional screening layer models.

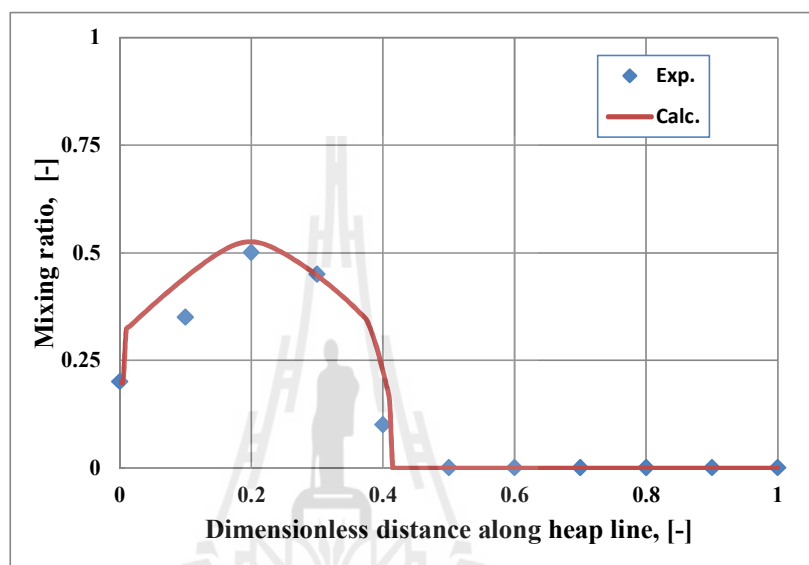


Figure 17. Validation of three-dimensional screening layer model
by fitting experimental data

Table 5. Operational and flowability parameters used in 3D model validation

Parameter	Value
Initial mixing ratio of segregating component, [-]	0.2
Feed rate on net volume basis, [cm ³ /s]	30
Total thickness of flowing layer, [cm]	0.5
Length of heap line, [cm]	30
Inclination angle of heap surface, [degree]	30
Feeder opening, [cm]	5
Penetration rate of segregating component, [cm/s]	0.032
Velocity ratio of separated to framing components, [-]	0.15
Packing rate of segregating component, [cm/s]	0.01
Void fraction of remained sub-layer, [-]	0.4
Void fraction of segregating sub-layer, [-]	0.35
Void fraction of separated sub-layer, [-]	0.4

4.2.2 Effect of process parameters on segregation of binary mixture

Definition of operational and flowability parameters

The effects of process parameters on segregation behavior of binary mixture are investigated using the two-dimensional screening layer model. The operational and flowability parameters are summarized in Table 6.

Table 6. Operational and flowability parameters used in study on effect of process parameters on segregation of binary mixture

Parameter	Value
Initial mixing ratio of segregating component, [-]	0.2
Feed rate on net volume basis, [cm ³ /s]	42
Total thickness of flowing layer, [cm]	0.5
Length of heap line, [cm]	30
Width of apparatus, [cm]	10
Penetration rate of segregating component, [cm/s]	0.10
Velocity ratio of separated to framing components, [-]	0.2
Packing rate of segregating component, [cm/s]	0
Void fraction of remained sub-layer, [-]	0.5
Void fraction of segregating sub-layer, [-]	0.5
Void fraction of separated sub-layer, [-]	0.5

Typical profiles of mixing ratio and flowing sub-layer thicknesses

Figure 18 shows the variation of distribution of mixing ratio of segregating component with time. The peak value of the mixing ratio increases and the segregation zone becomes wider for longer descending time.

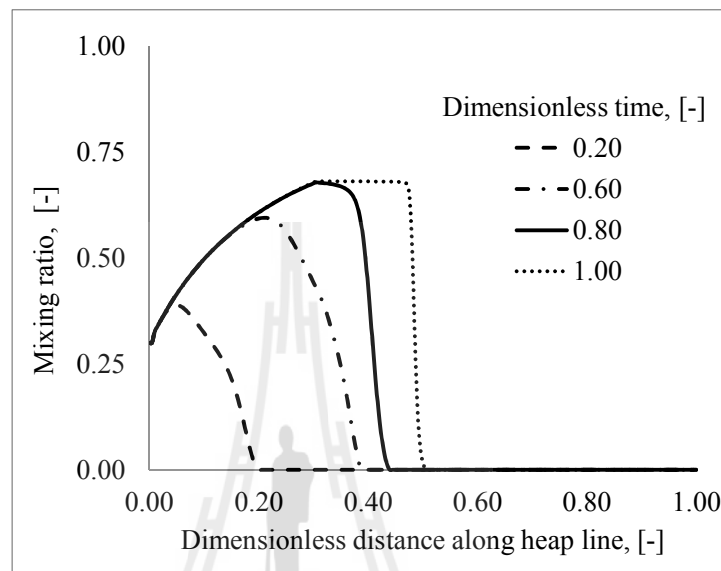


Figure 18. Variation of mixing ratio with time

Figures 19 (a), (b) and (c) illustrate the variation of thicknesses of flowing sub-layers with time. The thickness of the segregating layer declines and the thicknesses of the separated and remained layers increase with time as fine particles separate from the segregating layer and join the separating one and the coarse particles ally with the remained layer.

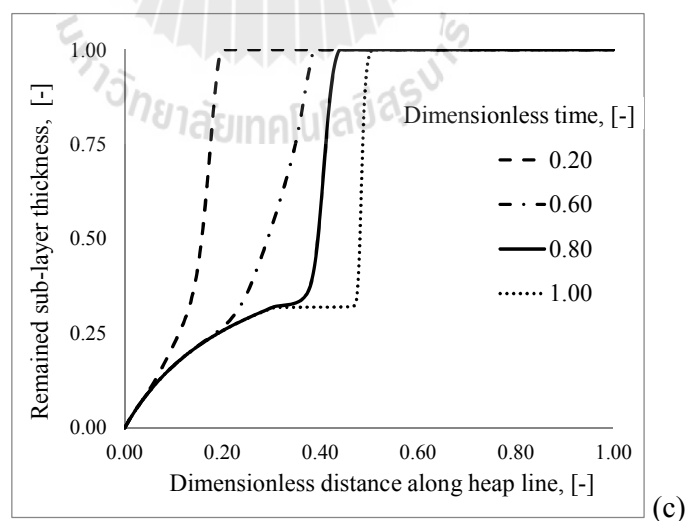
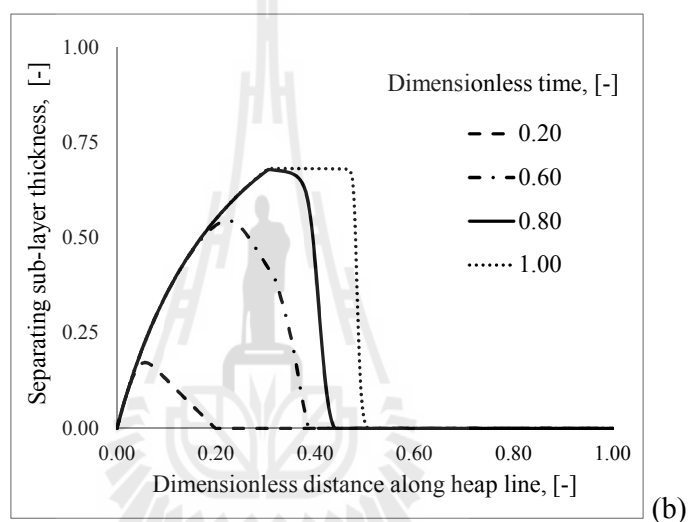
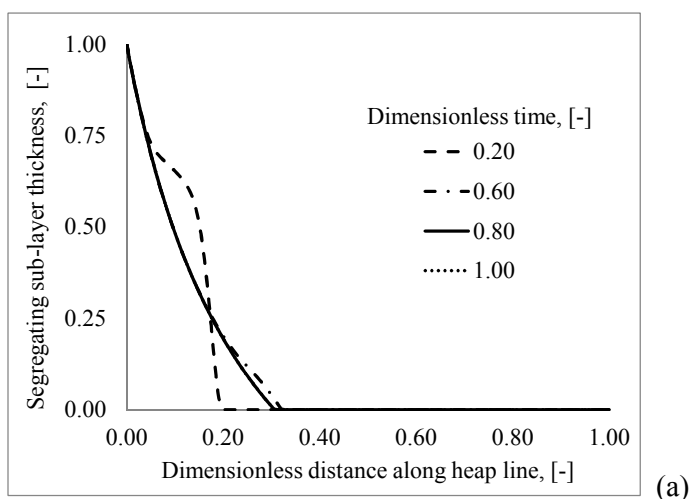


Figure 19. Variation of thicknesses of flowing sub-layers with time:
 (a) segregating, (b) separating, (c) remained.

Effect of penetration and packing rates

Figure 20 illustrates the effect of penetration rate on the mixing ratio profile along the heap line. Segregation is more profound at higher penetration rate with fine particles concentrating close to the heap center. The distribution is almost uniform at the low penetration rate of 0.01 cm/s corresponding to the well-mixed particle mixture with low degree of segregation.

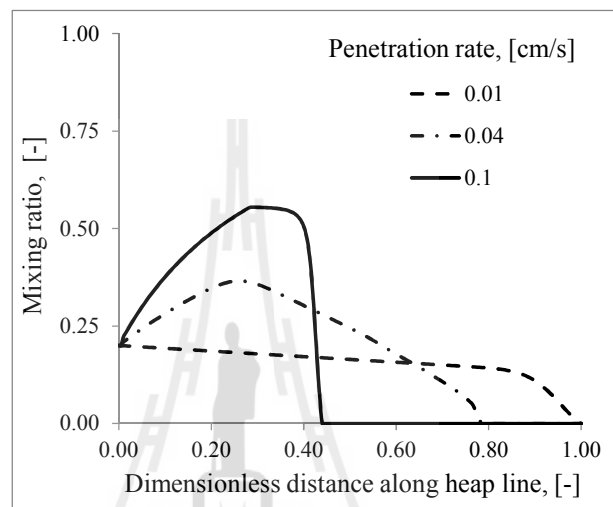


Figure 20. Effect of penetration rate on segregation profile

The effect of packing rate on segregation profile is shown in Fig. 21. The fine particles deposit into void spaces among course particles of static sub-layer slightly closer to the heap center at the higher packing rate than at the lower one.

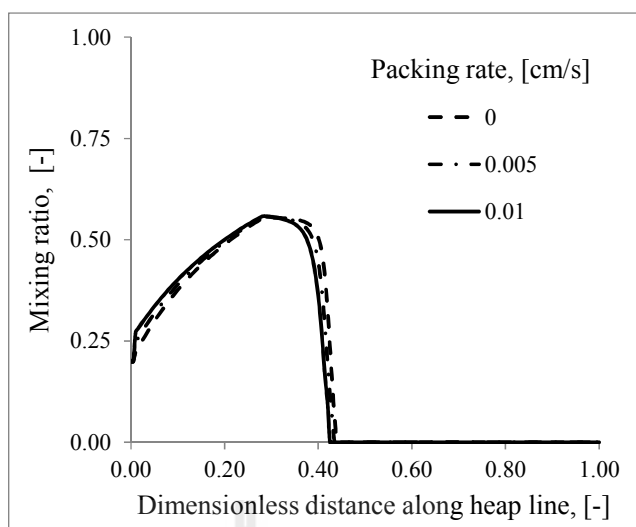


Figure 21. Effect of packing rate on segregation profile

Effect of velocity ratio

Figure 22 illustrates the effect of velocity ratio on segregation profile. The fine particles separate more easily from the particle mixture at the low velocity ratio.

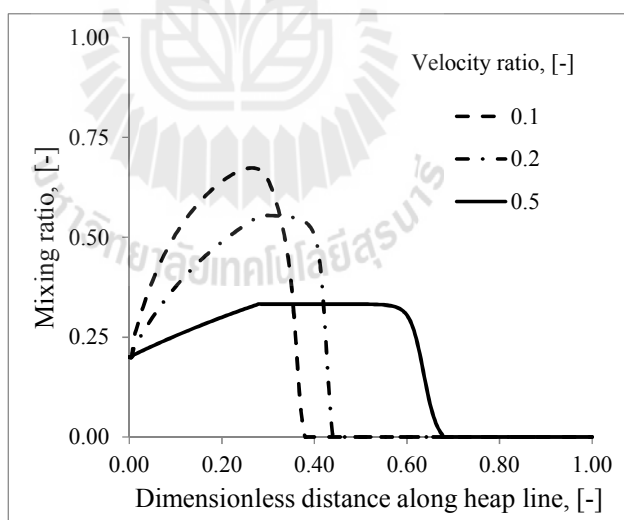


Figure 22. Effect of velocity ratio on segregation profile

Influence of operational parameters

The effect of the initial mixing ratio on segregation profile is illustrated in Fig. 23. The fine particles separate more easily from mixture of low initial mixing ratio of segregating component yielding the narrow segregation zone and high peak value.

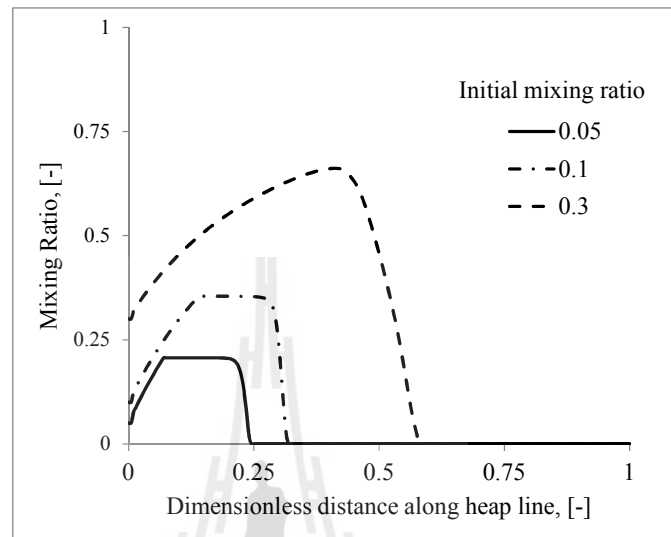


Figure 23. Effect of initial mixing ratio on segregation profile

Figure 24 illustrates the effect of feed rate on segregation profile. The maximum value of fine component is high and the segregation zone is narrow at the low feed rate. The fine particles are dragged by coarse particles during descending along the heap and there are fewer chances for them to separate at the high flow rate.

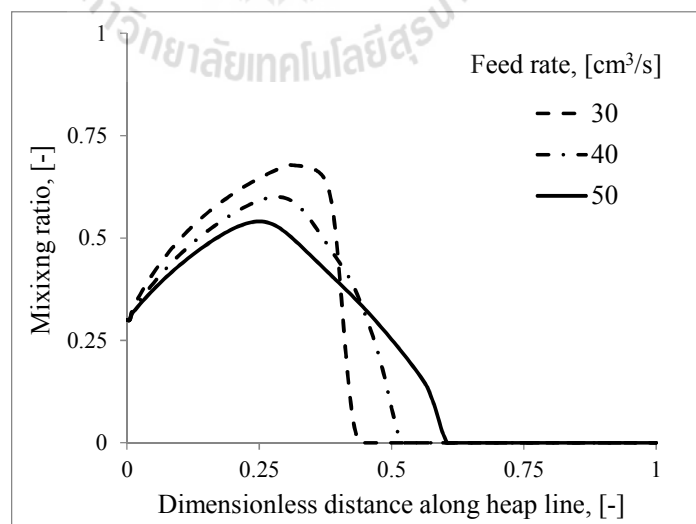


Figure 24. Effect of feed rate on segregation profile

Influence of hopper geometry parameters

The effect of hopper dimension on segregation of binary mixture was simulated by varying the length of heap line. Segregation in the wider hopper with longer heap line is more significant than in the narrow one. The narrow segregation zone with higher peak value is observed for the heap line of 30 cm, as shown in Fig. 25. Fine particles have more chances to separate from the particle mixture in the segregating sub-layer during flow along the longer heap path than the shorter one.

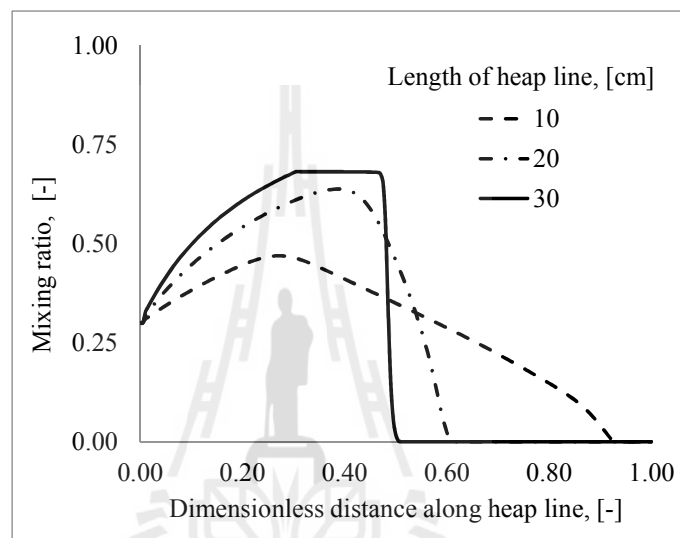


Figure 25. Effect of length of heap line on segregation profile

4.2.3 Comparison of segregation patterns in two and three dimensions

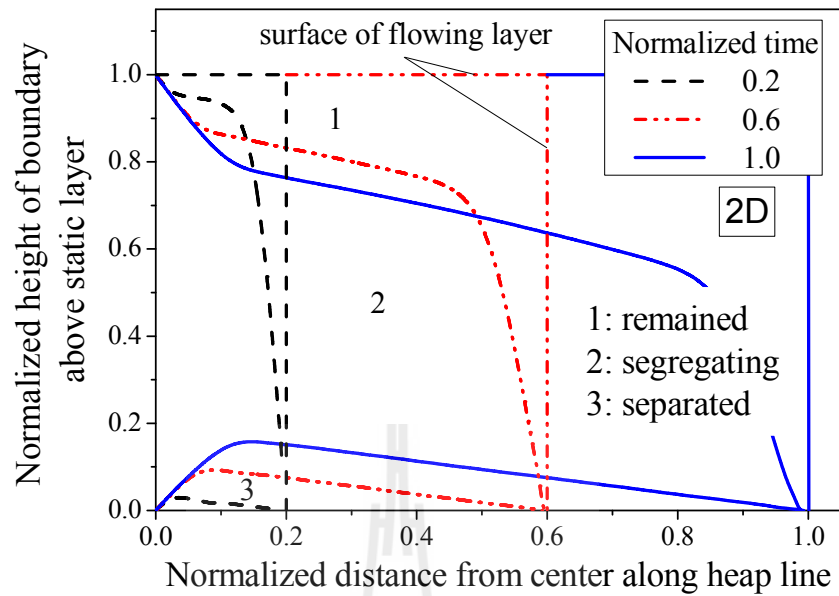
The typical values of operational and flowability parameters used in the comparison of segregation patterns in two and three dimensions are summarized in Table 7.

Figure 26 illustrates the composition of different sub-layers at various times calculated using two- and three-dimensional models. The intermediate segregating sub-layer by the three-dimensional model is depleted with small particles and divided on separated and remained sub-layers at shorter distance from the heap center in comparison with one by the two-dimensional model. This difference is more profound for a longer time. The descending sub-layer velocity decreases along the heap line in

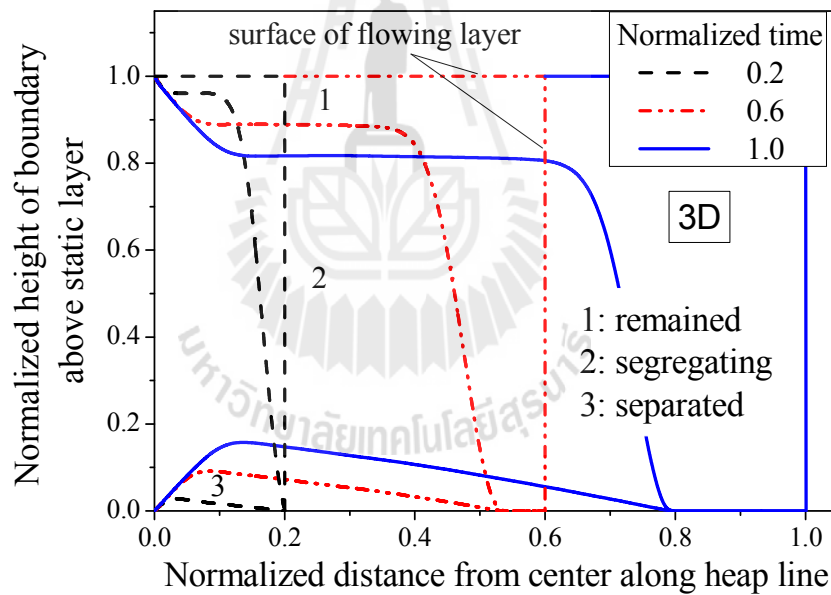
the three-dimensional case due to the expansion of flowing zone giving more chances for small particles to penetrate through the segregating sub-layer to the separated one.

Table 7. Operational and flowability parameters used in comparison of two and three dimensional data

Parameter	Value
Initial mixing ratio of segregating component, [-]	0.3
Feed rate on net volume basis, [cm ³ /s]	20
Total thickness of flowing layer, [cm]	0.3
Length of heap line, [cm]	30
Inclination angle of heap surface, [degree]	30
Depth of apparatus, [cm] (2D)	3
Feeder opening, [cm] (3D)	0.8
Penetration rate of segregating component, [cm/s]	0.05
Velocity ratio of separated to framing components, [-]	0.1
Packing rate of segregating component, [cm/s]	0.01
Void fraction of remained sub-layer, [-]	0.4
Void fraction of segregating sub-layer, [-]	0.35
Void fraction of separated sub-layer, [-]	0.4



(a)



(b)

Figure 26. Variation of sub-layer thicknesses with time by (a) 2D and (b) 3D models

The effect of penetration rate Q on the segregation pattern is shown in Fig. 27. The segregation is more pronounced at higher value of penetration rate as the segregation zones get narrow in both two- and three-dimensional cases and in the three-dimensional case this effect is more evident.

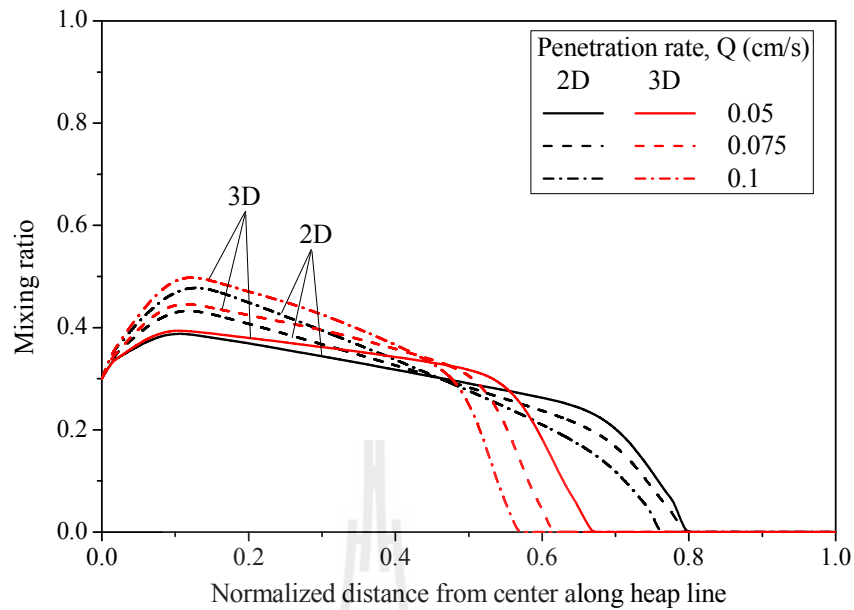


Figure 27. Effect of penetration rate on segregation pattern

The effect of the initial mixing ratio on the segregation pattern is illustrated in Fig. 28. With increasing mixing ratio at constant total thickness of the flowing layer, the segregation zone expands as there will be more small particles that could flow further along the heap line.

The correlation is shown in Fig. 29 for the penetration rates in two- and three-dimensional cases calculated by Eq. (76) for various initial mixing ratios using A , B , p constant values specified in each dimension by fitting experimental data [Shinohara *et.al.*, 1972, Shinohara K. and Enstad G., 1972]. The penetration rate in the three-dimensional case is higher than one in the two-dimensional case due to expanding free surface, which yields the narrower segregation zone, that is, higher degree of segregation.

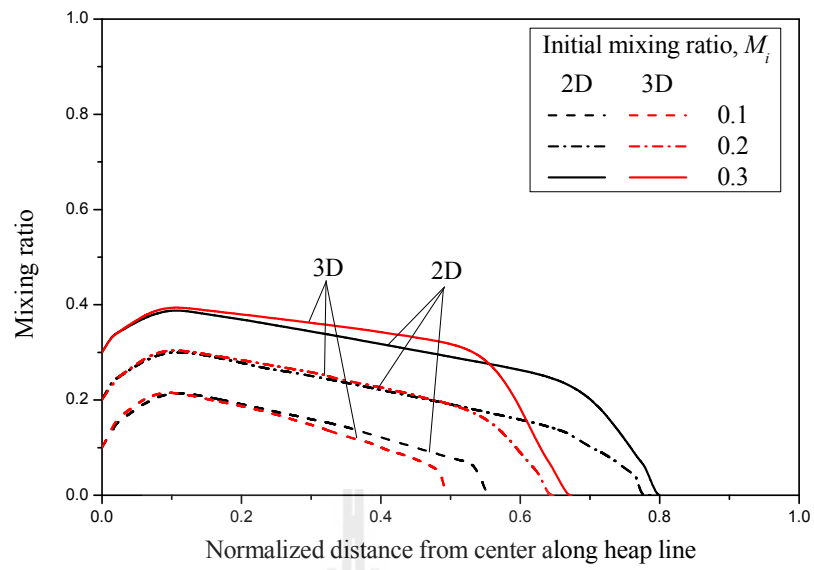


Figure 28. Variation of segregation patterns with initial mixing ratio

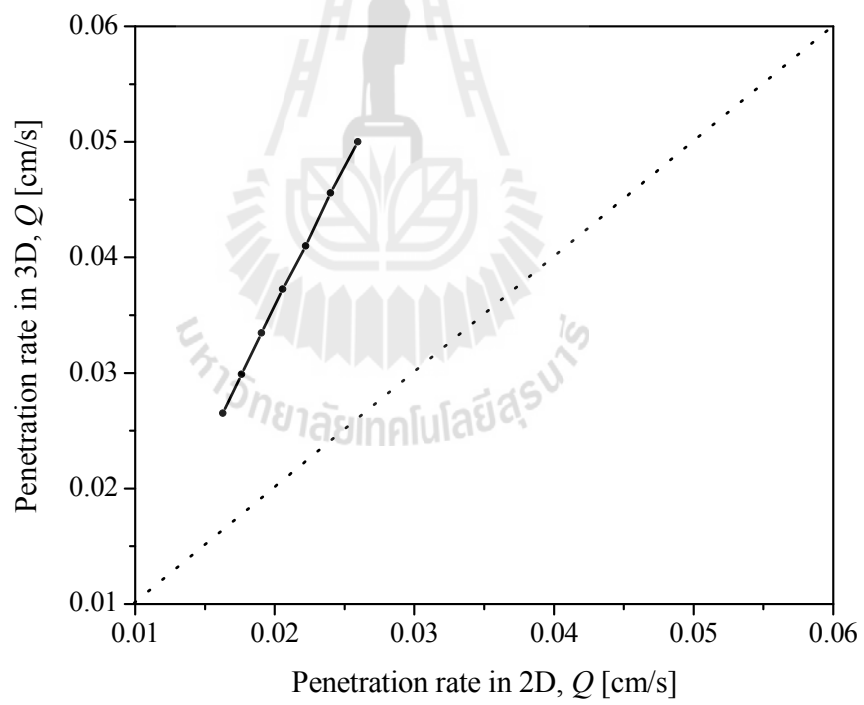


Figure 29. Correlation of penetration rates in 3D and 2D

5. Conclusion

The segregation mechanisms of binary-sized particle mixtures were investigated in filling hoppers.

The discrete element method was applied successfully for generation of segregation patterns during heap formation. Segregation profiles simulated by DEM were similar to ones obtained in experiments as well as calculated by the screening layer model. Thus, the applicability of DEM models was confirmed for generation of data to be used in the analysis of segregation mechanism in industrial apparatus.

The effects of particle mixture properties, process parameters, material properties and hopper geometry were investigated on the extent of segregation using the screening layer model. The segregation zone was found to be narrow for low initial mixing ratio and mixture feed rate, for longer heap flow length with higher penetration rate.

The detailed comparison of segregation patterns generated during heap formation in filling the two- and three-dimensional vessels with binary-sized particle mixture was carried out using the screening layer model. The segregation patterns and related characteristics like flowing zone size and velocity profiles are calculated and visualized with the developed programs.

The segregation was confirmed to be more profound in the case of the three-dimensional heap in comparison with the two-dimensional one as sub-layer velocities decrease during flowing down the conical heap as a result of expansion of flowing surface giving small segregating particles more chances for penetration.

The results of the present analysis are intended to be used for understanding the segregation mechanism in filling the hopper and get the design guide in various industrial processes.

Partial results of the present research were presented at the international conference, 5th Asian Particle Technology Symposium APT2012, on 2-5 July 2012 in Singapore and were published in peer-reviewed proceedings (B. Golman and K. Shinohara, Analysis of heap segregation in filling vessels, Proc. of the 5th Asian Particle Technology Symposium APT2012, pp. 231-236).

References

- Bates L., User guide to segregation, in Hayes G., Ed., British Materials Handling Board, Marlow, U. K., 1997.
- Bridgwater J., Sharpe N.W. and Stocker D.C., Particle mixing by percolation. *Chemical Engineering Research and Design*, **47**, 114-119, 1969.
- Bridgwater J. and Ingram N.D., Rate of spontaneous inter-particle percolation, *Chemical Engineering Research and Design*, **49**, 163-169, 1971.
- Campbell H. and Bauer W.C., Cause and cure of demixing in solid–solid mixers, *Chemical Engineering*, 179-185, 1966.
- Cleary P.W., Predicting charge motion, power draw, segregation and wear in ball mills using discrete element methods, *Minerals Engineering*, **11**, 1061-1080 , 1998.
- Cleary P.W., DEM simulation of industrial particle flows: Case studies of dragline excavators, mixing in tumblers and centrifugal mills, *Powder Technology*, **109**, 83-104, 2000.
- Cundall P.A. and Strack O.D.L, A discrete numerical model for granular assemblies, *Geotechnique*, **29**, 47-65, 1979.
- Fan Y., Boukerkour Y., Blanc T., Umbanhowar P.B., Ottino J.M. and Lueptow R.M., Stratification, segregation, and mixing of granular materials in quasi-two-dimensional bounded heaps, *Phys. Rev. E*, **86**, 051305, 12 p., 2012.
- EDEM 2.5 user's manual, DEM Solutions, Edinburgh, Scotland, 2013.
- Hairer E. and Wanner G., Solving ordinary differential equations II: Stiff and differential-algebraic problems, 2 ed., Springer Verlag, Berlin, 1996.
- Hoffmann A.C., Janssen L.P. and Prins J., Particle segregation in fluidized binary mixtures, *Chemical Engineering Science*, **48**, 1583-1592, 1993.
- Gantt J.A. and Gatzke E.P., High-Shear granulation modeling using a discrete element simulation approach, *Powder Technology*, **156**, 195-212, 2005.
- Garg R., Galvin J., Li T. and Pannala S., Open-source MFI-X-DEM software for gas-solids flows: Part I–verification studies, *Powder Technology*, **220**, 122-137, 2012.
- Gear C.W., Numerical Initial Value Problems in Ordinary Differential Equations,

- Prentice Hall, 1971.
- Gray J., Particle size segregation in granular avalanches: A brief review of recent progress,” in *IUTAM-ISIMM Symposium on Mathematical Modeling and Physical Instances of Granular Flows*, edited by J. Goddard, J.Jenkins, and P. Giovine, AIP, Melville, NY, Vol. **1227**, pp. 343-362, 2010.
- Ketterhagen W.R. and Hancock B.C., Optimizing the design of eccentric feed hoppers for tablet presses using DEM, *Computers and Chemical Engineering*, **34**, 1072-1081, 2010.
- Kruggel-Emden H., Simsek E., Rickelt S., Wirtz S., Scherer V., Review and extension of normal force models for the Discrete Element Method, *Powder Technology*, **171**, 157-173, 2007.
- Li H. and McCarthy J., Cohesive particle mixing and segregation under shear, *Powder Technology*, **164**, 58-64, 2006.
- Li Y., Xu Y. and Thornton C., A comparison of discrete element simulations and experiments for ‘sandpiles’ composed of spherical particles, *Powder Technology*, **160**, 219-228, 2005.
- Liss E.D., Conway S.L., Zega J.A. and Glasser B.J., Segregation of powders during gravity flow through vertical pipes, *Pharmaceutical Technology*, 78-96, 2004.
- Makse H.A., Cizeau P. and Stanley H.E., Possible stratification mechanism in granular mixtures, *Phys. Rev. Lett.*, **78**, 3298—3301, 1997.
- Marks B., Rognon P.G. and Einav I., Grainsize dynamics of polydisperse granular segregation down inclined planes, *Journal of Fluid Mechanics*, **1**, 1-13, 2011.
- McCarthy J.J., Turning the corner in segregation, *Powder Technology*, **192**, 137-142, 2009.
- Mishra B.K. and Rajamani R.J., The discrete element method for the simulation of ball mills, *Applied Mathematical Modeling*, **16**, 598-604, 1992.
- Mitchell D.R., Segregation in the handling of coal, *Transactions AIME*, **130**, 107-142, 1938.
- Prigozhin L., A variational problem of bulk solids mechanics and free-surface segregation, *Chemical Engineering Science*, **48**, 3647 - 3656, 1993.
- Rahman M., Shinohara K., Zhu H.P., Yu A.B. and Zulli P., Size segregation

- mechanism of binary particle mixture in forming a conical pile, *Chemical Engineering Science*, **66**, 6089–6098, 2011.
- Schiesser W. E. and Griffiths G. W. A Compendium of Partial Differential Equation Models: Method of Lines Analysis with Matlab. Cambridge University Press, 2009.
- Seaton T.W., Sand Segregation, *Metal Industry*, **22**, 67-72, 1960.
- Shinohara K. , Demitsu Y., Gotoh K. and Tanaka T. Mechanism of gravity flow of particles from a hopper, *Industrial Engineering Chemistry Process Design and Development*, **7**, 378–383, 1968.
- Shinohara K., Shoji S. and T.Tanaka, Mechanisms of segregation and blending of particles flowing out of mass-flow hoppers, *Industrial Engineering Chemistry Process Design and Development*, **9**, 174-180, 1970.
- Shinohara K., Shoji K. and Tanaka T. Mechanism of size segregation of particles in filling a hopper, *Industrial Engineering Chemistry Process Design and Development*, **11**, 369–376, 1972.
- Shinohara K. and Miyata S. Mechanism of density segregation of particles in filling vessels. *Industrial Engineering Chemistry Process Design and Development*, **23**, 423–428, 1984.
- Shinohara K. and Enstad G., Segregation mechanism of binary solids in filling axi-symmetric hoppers, In: *Proceedings of the Second World Congress Particle Technology*, Kyoto, 45–52, 1990.
- Shinohara K. and Saitoh J. Mechanism of solids segregation over a two-dimensional dead man in a blast furnace, *ISIJ International*, **33**, 672-680, 1993.
- Shinohara K., Golman B. and Nakata T., Size segregation of multicomponent particles during filling of a hopper, *Advanced Powder Technology*, **12**, 33-43, 2001.
- Shinohara K., Golman B. and Mitsui T., Segregation pattern of multi-component particles of different densities during the filling of hopper, *Powder Handling Processing*, **14**, 91-95, 2002.
- Shinohara K. and Golman B., Particle segregation of binary mixture in a moving bed by penetration model, *Chemical Engineering Science*, **57**, 277–285, 2002.
- Shinohara K. and B.Golman, Density segregation during solids handling in a

- two-dimensional hopper, *Advanced Powder Technology*, **14**, 333-347, 2003.
- Shinohara K., Segregation of particles, in: H. Masuda et al. (Eds.) *Powder Technology Handbook*, CRC Press, 2006.
- Shinohara K., Satoh K., Xie H. and Golman B. Segregation pattern of binary particle mixture in moving bed of blast furnace model, *Bulk Solids & Powder Science & Technology*, **2**, 1-5, 2007.
- Silva S.R.D., Dyroy A. and Enstad G.G., Segregation mechanisms and their quantification using segregation testers, in: A.D. Rosato, D.L. Blackmore (Eds.), *Segregation in Granular Flows*, Kluwer Academic Press, 11–29, 2000.
- Tang P. and Puri V. M., Methods for minimizing segregation: A review, *Particulate Science and Technology*, **22**, 321-337, 2004.
- Tatemoto Y., Mawatari Y., Yasukawa T. and Noda K., Numerical simulation of particle motion in vibrated fluidized bed, *Chemical Engineering Science*, **59**, 437 – 447, 2004.
- Williams J.C., The segregation of particulate materials. A review, *Powder Technology*, **15**, 245-251, 1976.

